NASA TECHNICAL NOTE

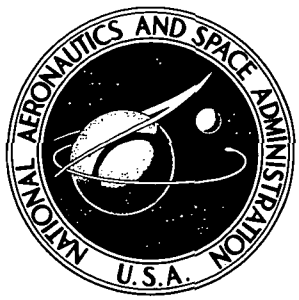

NASA TN D-7171

NASA TN D-7171

FISSION-GAS RELEASE FROM URANIUM NITRIDE AT HIGH FISSION-RATE DENSITY

by Michael B. Weinstein, Thomas A. Kirchgessner, and Thomas N. Tambling

Lewis Research Center
Cleveland, Ohio 44135

NATIONAL AERONAUTICS AND SPACE ADMINISTRATION • WASHINGTON, D. C. • MARCH 1973

1. Report No.	2. Government Accession No.	3. Recipient's Catalog No.
NASA TN D-7171		

4. Title and Subtitle	5. Report Date
FISSION-GAS RELEASE FROM URANIUM NITRIDE AT HIGH FISSION-RATE DENSITY	March 1973
	6. Performing Organization Code

7. Author(s)	8. Performing Organization Report No.
Michael B. Weinstein, Thomas A. Kirchgessner, and Thomas N. Tambling	E-7097
	10. Work Unit No. 503-05

9. Performing Organization Name and Address	11. Contract or Grant No.
Lewis Research Center National Aeronautics and Space Administration Cleveland, Ohio 44135	

12. Sponsoring Agency Name and Address	13. Type of Report and Period Covered
National Aeronautics and Space Administration Washington, D.C. 20546	Technical Note
	14. Sponsoring Agency Code

15. Supplementary Notes

16. Abstract

A sweep gas facility has been used to measure the release rates of radioactive fission gases from small UN specimens irradiated to 8-percent burnup at high fission-rate densities. The measured release rates have been correlated with an equation whose terms correspond to direct recoil release, fission-enhanced diffusion, and atomic diffusion (a function of temperature). Release rates were found to increase linearly with burnups between 1.5 and 8 percent. Pore migration was observed after operation at 1550 K to over 6-percent burnup.

17. Key Words (Suggested by Author(s))	18. Distribution Statement
Fission gas release Uranium nitride High fission rate	Unclassified - unlimited

19. Security Classif. (of this report)	20. Security Classif. (of this page)	21. No. of Pages	22. Price*
Unclassified	Unclassified	55	$3.00

* For sale by the National Technical Information Service, Springfield, Virginia 22151

Page Intentionally Left Blank

CONTENTS

FISSION-GAS RELEASE FROM URANIUM NITRIDE AT HIGH FISSION-RATE DENSITY

by Michael B. Weinstein, Thomas A. Kirchgessner, and Thomas N. Tambling

Lewis Research Center

SUMMARY

A sweep gas facility has been used to measure the release rates of radioactive fission gases from small UN specimens irradiated to 8-atom-percent fissions (burnup) at high fission-rate densities.

Fuel temperatures ranged from 600 to 1780 K. The measured gas release rates have been correlated with the predictions of a preliminary fission-gas transport-release model which includes atomic diffusion, fission-enhanced diffusion, and direct recoil release.

Radioactive-gas release rates were found to increase linearly with fission burnups between 1.5 and 8 percent.

Postirradiation photomicrographs show a high-temperature (>1500 K), high-burnup (6 percent) specimen to have large amounts of interconnected grain boundary porosity. Measured cesium-137 (Cs^{137}) releases from the high-temperature, high-burnup specimens can be approximately predicted by assuming that the gas is released to the grain boundaries.

Postirradiation photomicrographs after 6-percent burnup indicate that some bubble migration took place during operation at 1550 K.

INTRODUCTION

Efficient design of fuel elements for space power reactors depends in part on understanding the fission-gas release and transport processes in these power-producing fuel elements. As part of an effort to increase our knowledge of these processes, a program to measure fission-gas release rates from operating nuclear fuels was initiated at the NASA Lewis Research Center. This study has as a goal the development of a method to predict fission-gas release rates from uranium nitride (UN). The technique being used

is to measure radioactive fission-gas release rates from operating UN fuel specimens with a sweep gas facility and then to correlate these measured release rates with the test variables (temperature, fission-rate density, etc.) through a theoretical model.

The preliminary fission-gas transport-release model used in this study considers gas transport through the fuel by atomic and fission-enhanced diffusion (ref. 1), culminating in release of gas atoms from the surface. In this model, gas is also released by the recoil of gaseous fission fragments through the surface.

Carroll, in a pair of review papers (refs. 2 and 3), indicates that the fission-gas transport and release mechanisms are complex and, as yet, not completely understood. Possible fission-gas transport mechanisms include atomic diffusion, fission-enhanced diffusion, and gas bubble diffusion, all of which can be complicated by trapping and release processes.

Atoms diffusing through the fuel can be trapped by defects or by stationary gas bubbles. They can be released from these traps by defect annealing or by kinetic resolution from the bubbles. Similarly, bubbles diffusing under the influence of a driving force, such as a temperature gradient, may be trapped or delayed by solid fission product precipitates, dislocations, or grain boundaries. Release from these traps occurs when the driving force exceeds the retarding force.

These transport-trapping processes are themselves the product of multiple causes. As an example, Carroll (ref. 2) points out that possible bubble motion mechanisms are surface diffusion, volume (or bulk) diffusion, and evaporation-condensation. Domination of one bubble diffusion mechanism over the others depends on the material properties, the fuel temperature, and the bubble size (Nichols, ref. 4).

Fission-gas release mechanisms include direct recoil (the ejection of fission-produced atoms from the fuel), knockout (ref. 5) (the ejection of gas and fuel atoms from the fuel surface by recoiling fission fragments), as well as the release when diffusing gas atoms or bubbles reach a free surface. Free surfaces include internal cracks or grain boundaries open to the exterior surface of the fuel.

The tests reported herein were conducted to study the effects of three major variables on fission-gas release. The variables are temperature, fission-rate density, and burnup.

Small-size, high-enrichment UN samples were irradiated at high fission-rate densities to achieve high burnups (over 6 percent) in a reasonable length of time. Fuel temperatures ranged from 600 to 1780 K.

Based on the diffusion transport model chosen (atomic plus fission-enhanced diffusion with desorption and recoil release), equations were developed which relate measured fission-gas release rates to the test variables. Unknown constants in these equations were evaluated from the data.

TEST APPARATUS

The irradiation tests described in this report were conducted using a sweep gas facility located at the NASA Plum Brook Reactor Facility. A concise description of the sweep gas facility, as well as the design of the fuel pin and the irradiation capsule, is presented here. More detailed descriptions can be found in reference 6.

Sweep Gas Facility

The sweep gas facility is basically a helium flow system which provides a means of monitoring the fission-gas release from power-producing fuel samples. A simplified flow schematic of the sweep gas facility is shown in figure 1. Bottle-supplied helium is

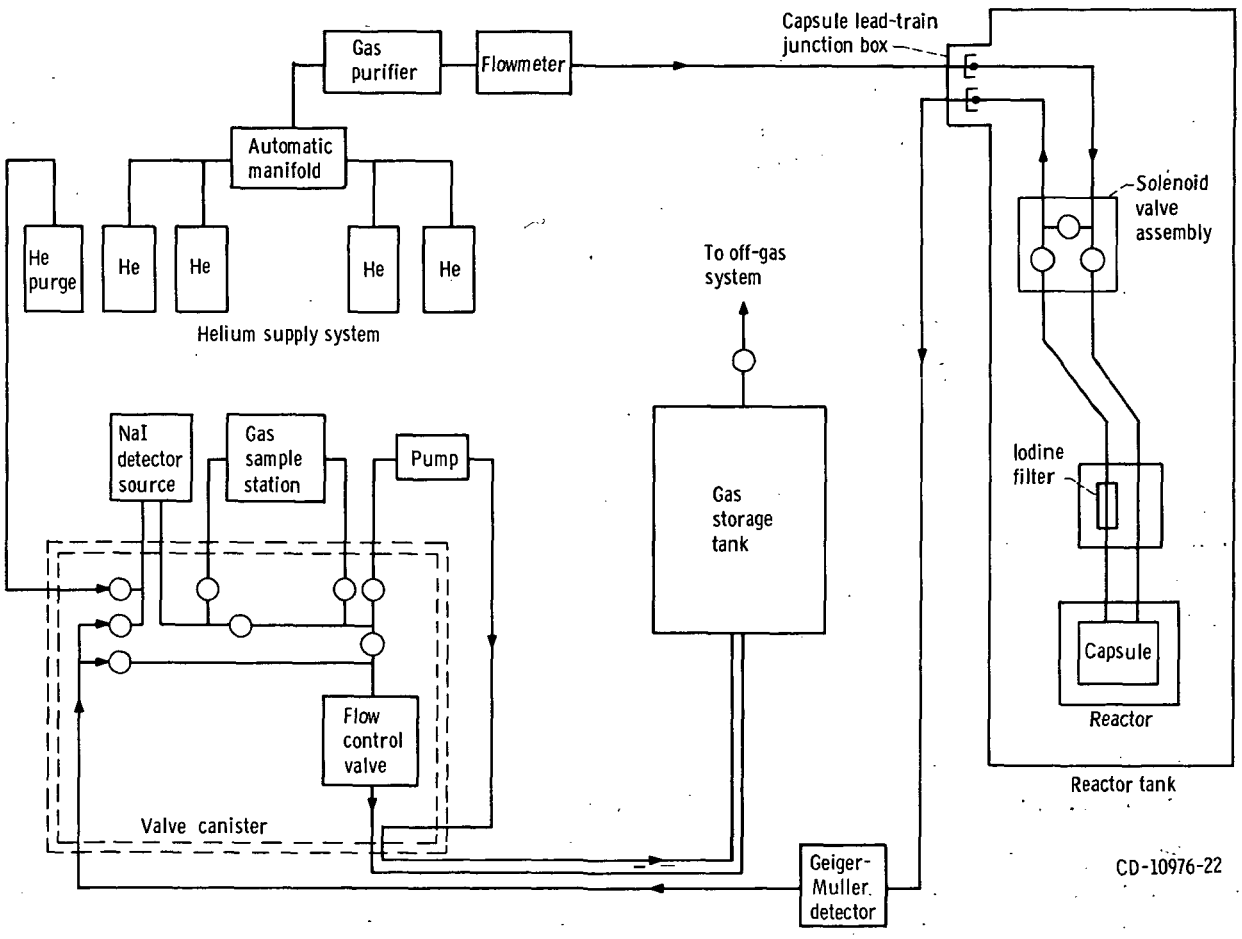

Figure 1. - Simplified schematic of sweep gas facility.

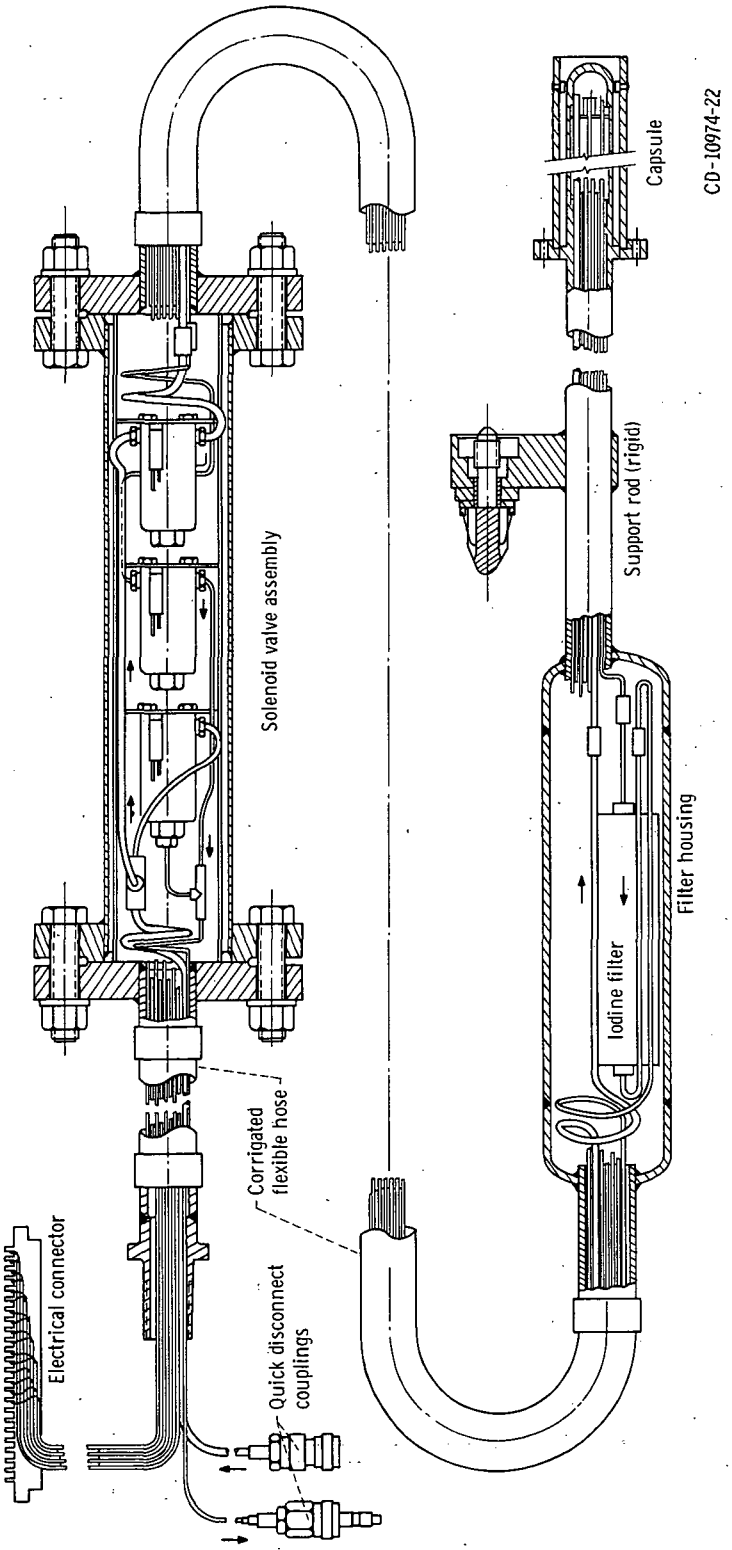

Figure 2. - Instrument lead system.

piped through a gas dehumidifier-purifier, a flowmeter, and an irradiation capsule containing a fuel specimen. Gaseous fission products released from the fuel sample are swept out of the capsule by the helium through a copper wool filter (to remove fission-produced iodine) and past a sodium iodide (NaI) scintillation detector, where the activity is measured. Samples of the sweep gas can be removed for more detailed analysis. After flowing past the detector, the gases are stored in a large tank for intermediate holding and radioactive decay before release to the reactor off-gas cleanup system.

The portion of the sweep gas facility located inside the reactor tank consists of an instrument lead system (fig. 2) containing the irradiation capsule, the iodine filter, and the solenoid valve assembly, plus the capsule insertion device. The entire instrument lead system is replaced as a unit with each new fuel specimen.

Irradiation Capsule

The small-volume irradiation capsule presently being used is shown in figure 3. It is designed to irradiate small-diameter fuel cylinders contained in a vented pin.

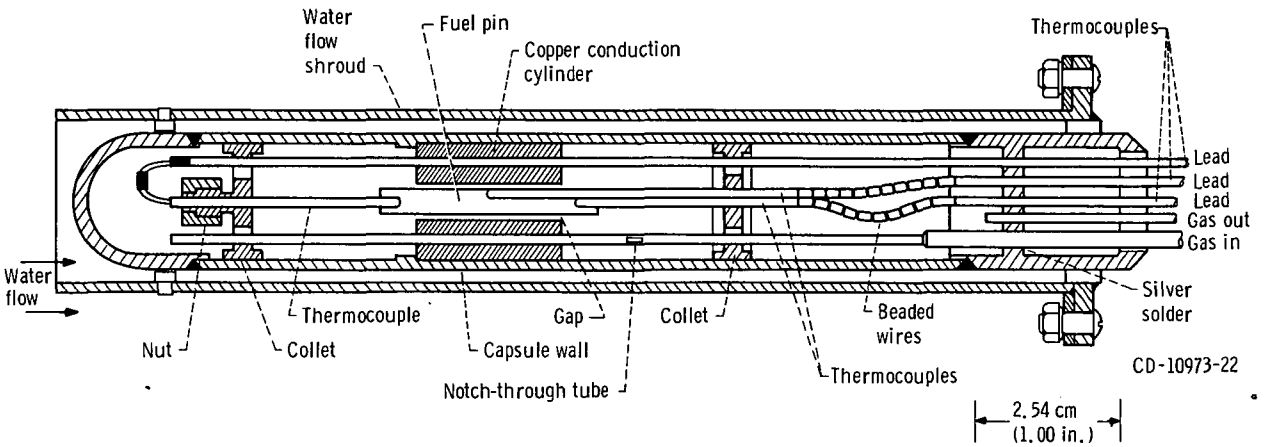

Figure 3. - Irradiation capsule.

The fuel sample is contained in a cylindrical molybdenum - 5-percent-titanium - 0.08-percent-zirconium (TZM) pin (fig. 4) which is vented at the upper end to permit the escape of fission gases into the helium sweep gas.

The fuel pin is axially supported and centered in the capsule by means of thermocouple sheathing tubes (molybdenum) attached at each end of the pin. A third thermocouple is set in a slot machined in the TZM clad. This latter thermocouple senses the

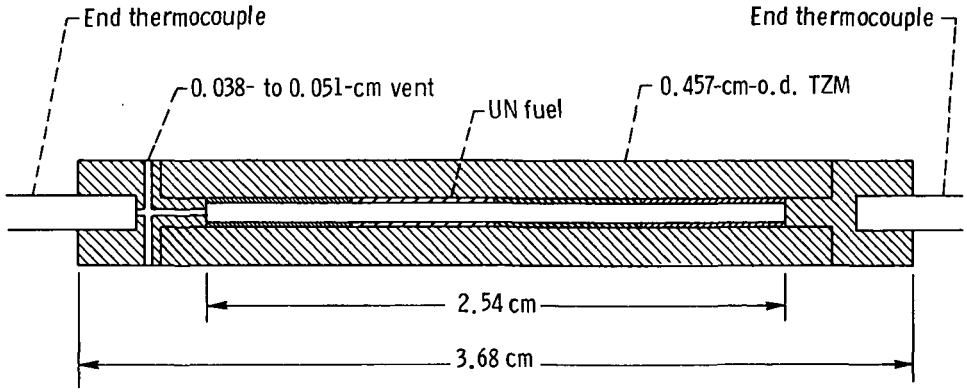

Figure 4. - Fuel pin assembly.

clad temperature midway along the pin.

The pin-capsule heat-transfer characteristics depend on the size of the gas gap between the pin and the copper conduction cylinder. Fuel temperature is primarily a function of fission power for a particular gap size.

Fuel Description

Each fuel pin irradiated in this program contained four UN pellets having the following nominal dimensions: 0.635 centimeter (0.25 in.) in length by 0.127 centimeter (0.05 in.) in outside diameter by 0.0763 centimeter (0.03 in.) in inside diameter. The total fuel length in each pin was approximately 2.54 centimeters (1.0 in.). The fuel pellets were fabricated at Oak Ridge National Laboratory by using the general procedure described in reference 7. Some modifications to these procedures were necessary because of the extremely small pellet diameters desired.

The steps in the fabrication procedure are as follows:

(1) Fully enriched (~93-percent U^{235}) UN powder is isostatically pressed into small rods.

(2) The rods are sintered at 2570 K for 2 hours in 1-atmosphere nitrogen (N_2) to a density of 13.3 g/cm^3 (93 percent of theoretical density).

(3) The sintered rods are centerless ground to a diameter of 0.127 centimeter (0.05 in.).

(4) The 0.0763-centimeter (0.03-in.) center hole is made by electrical discharge machining.

(5) After inspection, the pellets are vacuum annealed.

Pellet size is shown relative to a common pin in figure 5, and the typical fuel

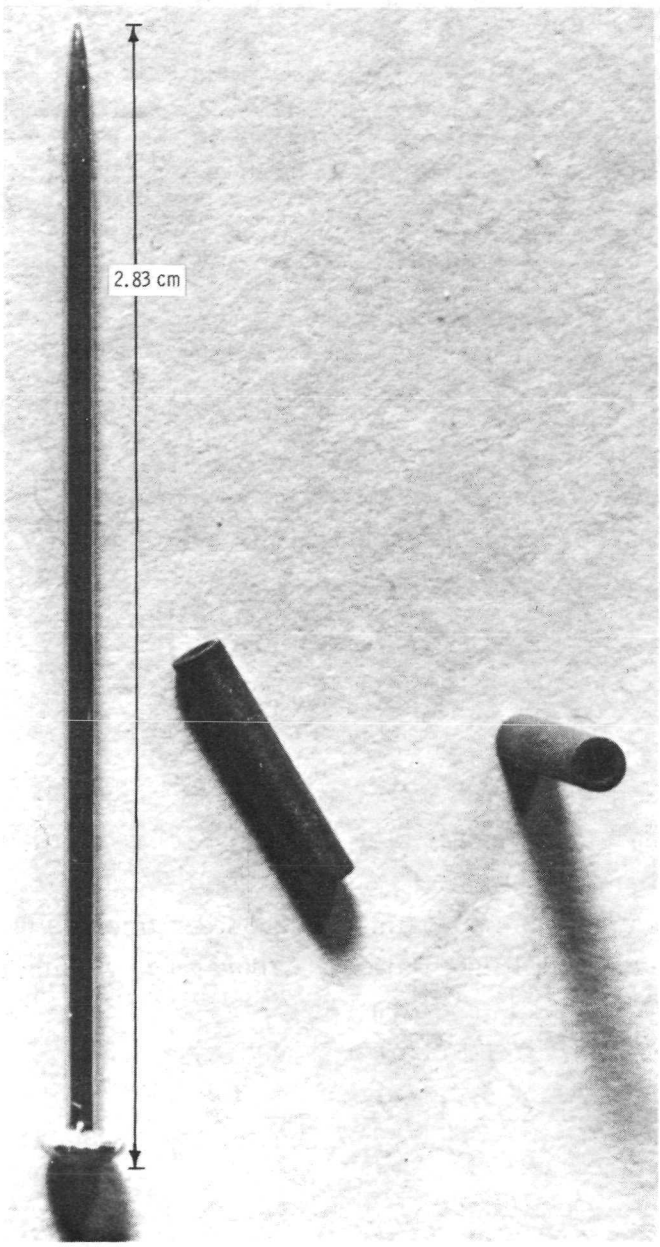

Figure 5. - Uranium nitride fuel pellets compared to 2.83-centimeter-long pin.

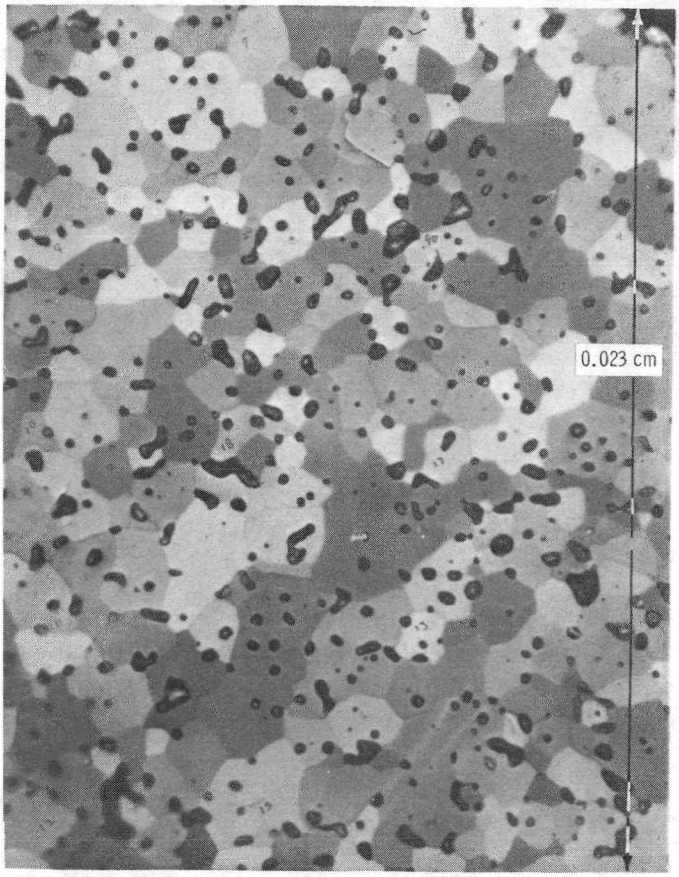

Figure 6. - Section of fuel pin before irradiation. X500.

microstructure is presented in figure 6. The typical physical, chemical, and isotopic characteristics of a pellet are as follows:

Fuel	UN
Nominal length, cm (in.)	0.635 (0.25)
Nominal outside diameter, cm (in.)	0.127 (0.05)
Nominal inside diameter, cm (in.)	0.0763 (0.03)
Percent density, percent of theoretical (theoretical density, 14.3 g/cm^3)	93
Oxygen concentration, ppm	450
Enrichment, percent of U^{235}	93
U^{236} content, percent	0.001
Grain size, cm	$\sim 1.5\times10^{-3}$

TEST PROCEDURES

All the irradiation tests discussed in this report were conducted in the following manner: During each 14- to 18-day Plum Brook reactor cycle, the fuel sample was irradiated at from one to six different temperatures with sweep gas pressure and flow rate held constant at all times.

The sweep gas flow rate was usually held at 0.2 cm^3/sec, so that the travel time from the capsule to the scintillation detector was 1130 seconds. This 1130-second travel time allowed the very short-lived fission-gas isotopes time to decay to an activity level too low to influence the scintillation detector data for the krypton and xenon isotopes studied (Kr^{87}, Kr^{88}, Kr^{85m}, and Xe^{135}).

Each constant-temperature (±10 K) run lasted from 24 to 48 hours, which was enough time for the release rates of the krypton isotopes to reach a quasi-steady state (release rate apparently unchanging in ~24 hours). Scintillation detector data were usually obtained every 6 hours (or less), and samples of the sweep gas were obtained every 3 to 7 days.

There was continuous (strip chart) recording of two of the fuel-pin-mounted thermocouples, as well as of the sweep gas flow rate. Hourly scans of all data channels were carried out automatically by the Plum Brook EDLAS (Experiment Data Logging and Alarm System).

At the end of the total irradiation period the in-tank capsule assembly was transported to the Plum Brook Hot Laboratory Facility for postirradiation examination. Included in this examination were

(1) Counting of capsule-mounted aluminum-cobalt wires for thermal fluence determinations

(2) Counting of capsule-mounted stainless-steel and nickel wires for fast fluence determinations

(3) Leaching of all internal capsule surfaces to detect vented uranium, cesium-137 (Cs^{137}), cerium-141 (Ce^{141}), and cerium-144 (Ce^{144})

(4) Neutron radiography of the fuel pin to detect possible gross fuel changes

(5) Fuel metallography to determine fuel density decreases and structural changes

(6) Determination of U^{236}/U^{235} ratios for burnup determination

(7) Fission product (Cs^{137}, Ce^{144}, Ce^{141}) counting to determine gross fission product retention in the fuel

GENERAL TEST HISTORIES

A concise description of the irradiation tests is presented in table I. Each of the

TABLE I. - OUTLINE OF IRRADIATION TESTS

Capsule	Total irradiation time, hr	Total burnup, percent	Primary test temperature, K	Temperature range (side thermocouple), K	Fission-rate density range, fissions/cm^3-sec	Number of sweep-gas samples
121	1294	8.3	1780	1215 to 1789	3.34×10^{14} to 8.29×10^{14}	9
122	1923	6.6	1223	593 to 1225	0.71×10^{14} to 3.64×10^{14}	19
123	1894	6.0	1505	579 to 1512	0.49×10^{14} to 4.45×10^{14}	19

three capsules was tested primarily at one fuel temperature, with shorter periods of time at other temperatures. Complete temperature-time plots are given in figures 7 to 9. The vertical lines on these plots represent temperature changes (planned or unplanned).

Thermal and fast fluences for each test are given in appendix A.

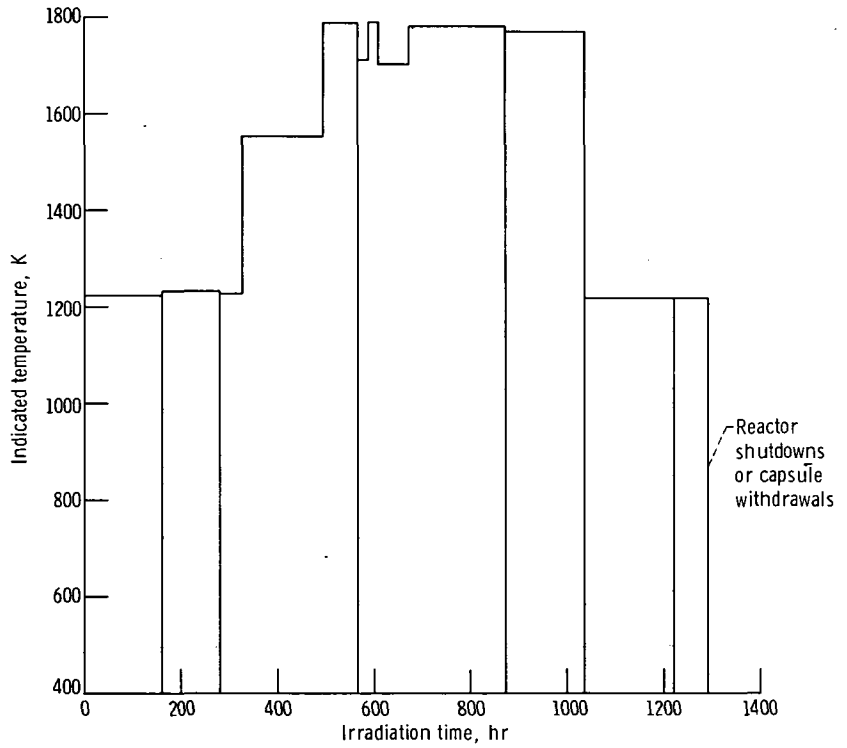

Figure 7. - Side thermocouple temperature as function of irradiation time - capsule 121. (Small variations not included.)

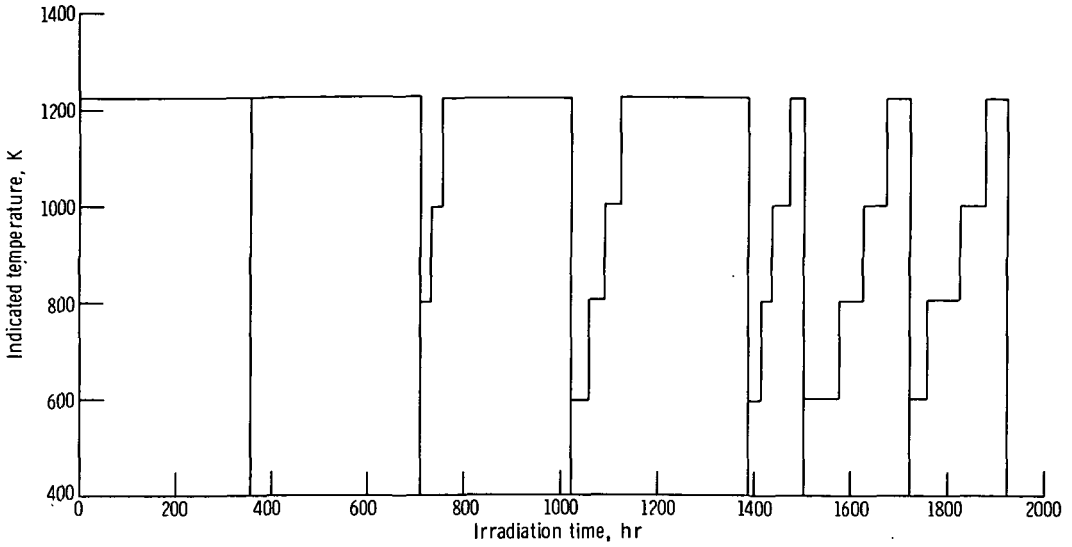

Figure 8. - Side thermocouple temperature as function of irradiation time - capsule 122. (Small variations not included.)

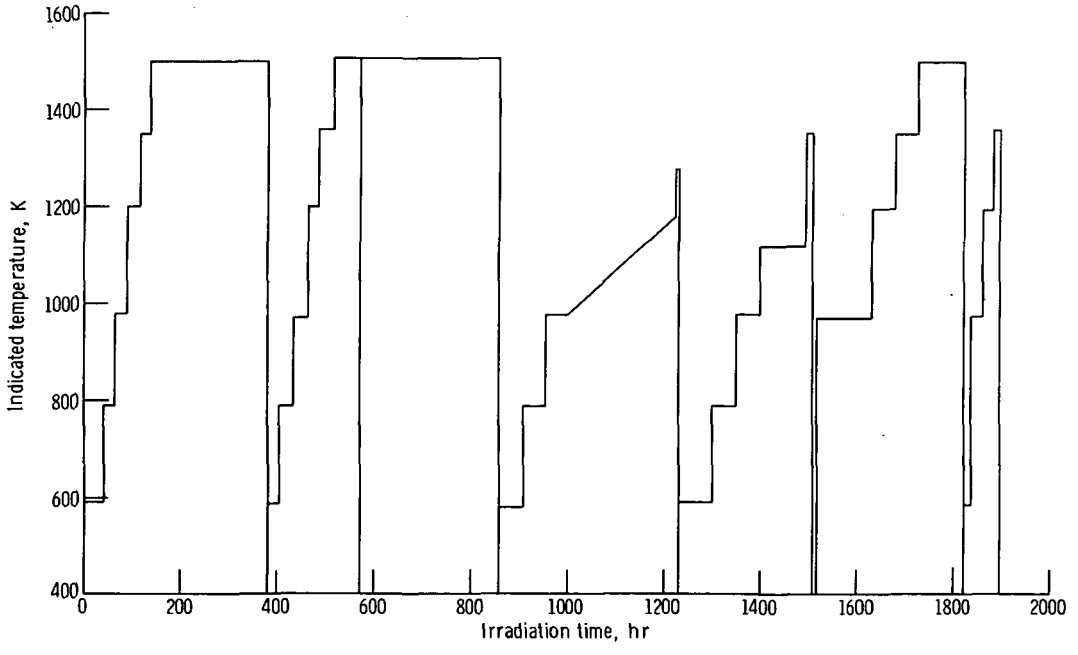

Figure 9. - Side thermocouple temperature as function of irradiation time - capsule 123. (Small variations not included.)

RESULTS AND DISCUSSION

Results

Our test and data-taking procedures are discussed in the section TEST PROCEDURES. Data reduction procedures and an extensive sampling of fission-gas release-rate data are presented in appendix B.

The release-rate data obtained in this series of irradiation tests can be correlated with a semiempirical model of fission-gas release which is based on concepts found in the literature. Test results and the correlation with the model are presented in this section.

Many of the results are primarily based on data obtained in the tests of capsule 123, although any conclusions are supported by data from the other tests (capsules 121 and 122; see table I).

Change in release rate with burnup. - The basic krypton-88[1] release rate data for capsule 123 are presented in figure 10 (similar data for capsules 121 and 122 can be found in appendix B). From the data in figure 10 it appears that, after about 1- to 1.5-percent burnup (3.2×10^{20} to 4.8×10^{20} fissions/cm^3), the release rate increases with burnup and that the rate of increase may be independent of test history.

A relation between release rate and burnup can be developed from the data in the following iterative manner: First, assume an approximate linear relation between release rate (or activity in the sweep gas) and burnup above 1.5 percent. This assumed relation is then used to group the data points in figure 10 in groups of constant burnup. Then the groups of data points at constant burnup but different temperatures are analyzed to obtain an average relation between release rate and temperature (table II), and this relation is then used to correct all the data points to a constant temperature (975 K).

The temperature correction is then applied to the original data points, all at different burnups; and the data are analyzed to determine the best linear fit in a least-squares sense between activity and burnup. If the least-squares relation is found to differ from the original guess, it is used to repeat the cycle.

When analyzed in this manner, the data in figure 10 yielded the linear relation

$$r = r_o(1 + 0.49\,b) \tag{1}$$

where the symbols are defined in appendix E.

The best-fit linear relation is shown in figure 11. All the data above a burnup of

---

[1]Krypton-88 is used for most of our analyses because its 2.4-MeV gamma ray is the easiest to monitor and count.

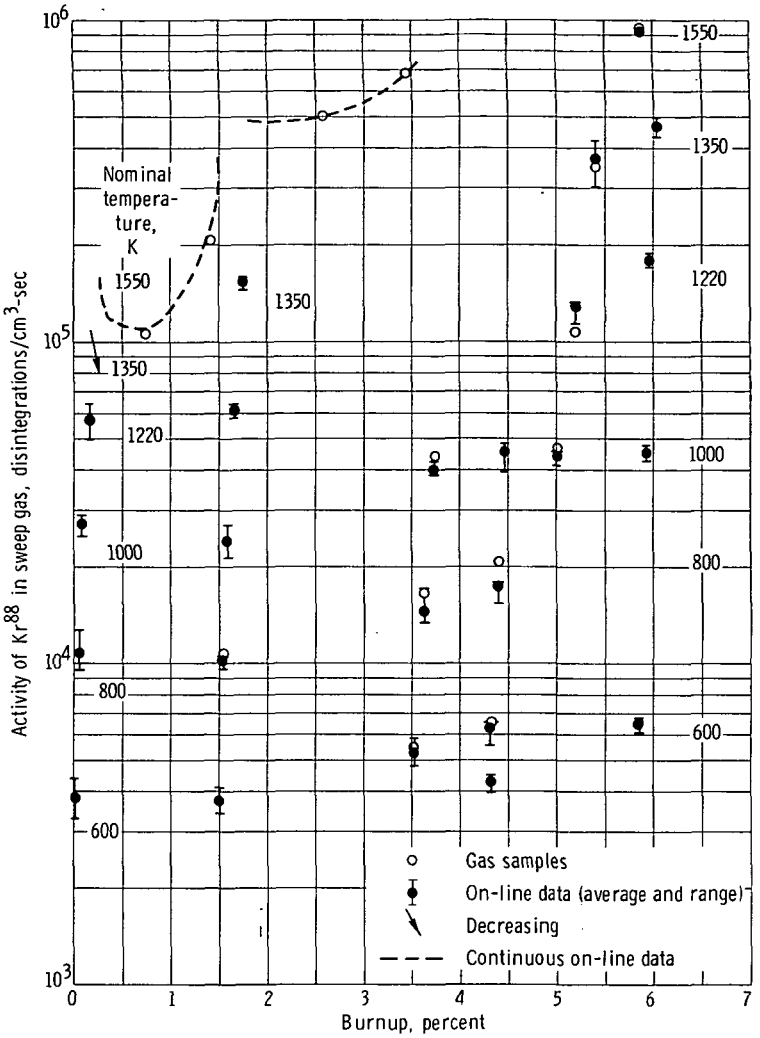

Figure 10. - Activity of krypton-88 as function of burnup - capsule 123.

TABLE II. - SWEEP GAS ACTIVITY AS FUNCTION OF TEMPERATURE

[Data for capsule 123.]

Side thermocouple temperature, K	Ratio of Kr^{88} activity at T to Kr^{88} activity at 975 K
586	0.149
790	.426
975	1.0
1197	2.83
1355	7.66
1504	18.3

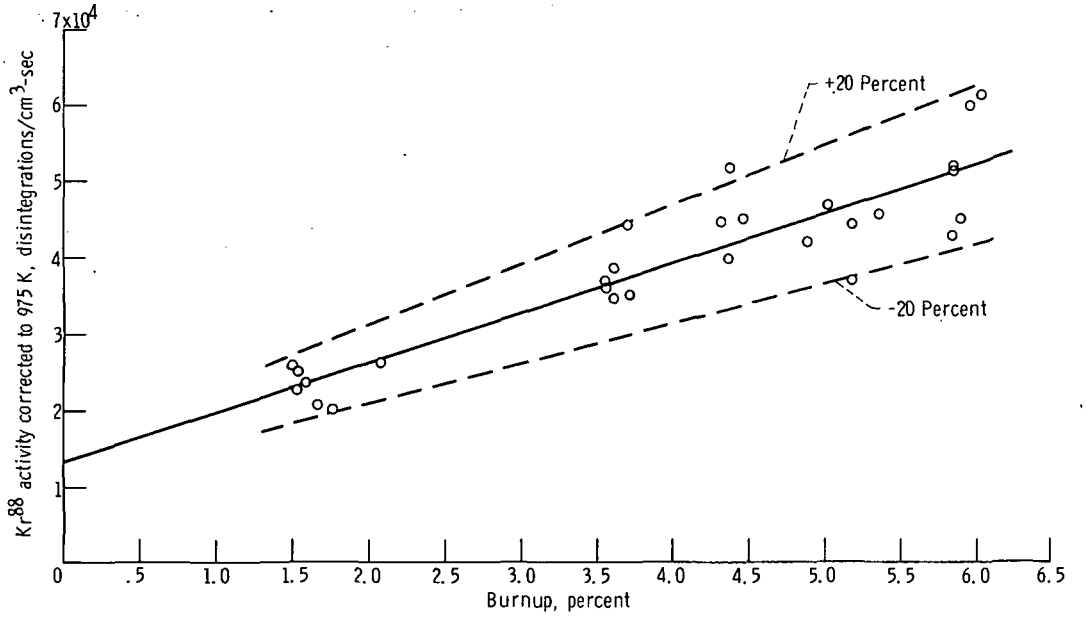

Figure 11. - Linear relation between release rate and burnup: activity of krypton-88 corrected to 975 K as function of burnup. Best fit: $r/r_0 = (1 + 0.49\ b)$.

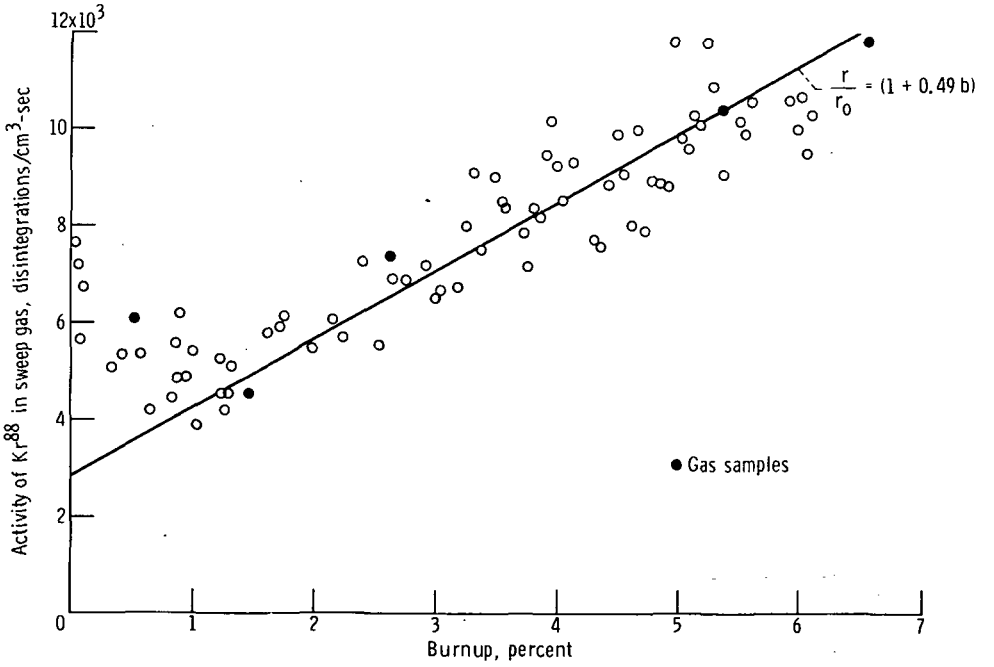

Figure 12. - On-line activity of krypton-88 as function of burnup - capsule 122. Nominal temperature, 1220 K.

1.5 percent in figure 10 are included. Almost all the data fall between limits of ±20 percent, and no consistent deviations with temperature were observed.

Data from capsule 122 at 1220 K also agree with equation (1) as shown in figure 12.

The low-burnup data (b < 2 percent) for all three capsules (figs. 10, 12, and appendix B) indicate a drop in release rate with increasing burnup to some minimum value prior to the beginning of the linear increase just discussed. A decreasing release rate has been observed by others (ref. 3, p. 566) and is generally explained as being caused by a decrease in surface area (refs. 3, 5, and 8) caused by surface smoothing or by sintering. We have also observed this effect during continuous irradiation at 800 K (fig. 13)[2]; so it is not caused only by high-temperature operation.

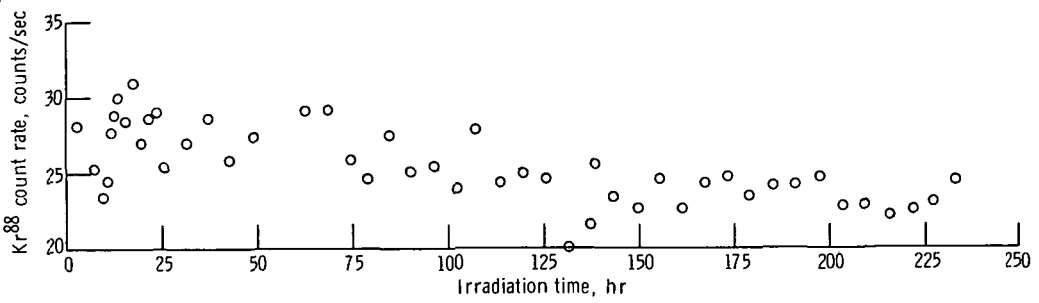

Figure 13. - Decrease in krypton-88 release rate with time from start of irradiation. Temperature of capsule 124, ~800 K.

Though observed, this decrease in release rate with increasing burnup during low-burnup operation will not be included in our correlation because the complete dependence on temperature, fission-rate density, and burnup is unknown.

Change in release rate with fission-rate density and temperature. - Based on the concepts of direct recoil of fission fragments, fission-enhanced diffusion (ref. 1), and atomic diffusion, an equation relating fission-gas release rates to fuel temperature and fission-rate density is

$$r = \frac{dYSLf}{4T} + fYS\left(\frac{D_{fo}f + D_o e^{-Q/RT}}{\lambda}\right)^{1/2} \qquad (2)$$

This equation was derived as equation (C8) in appendix C.

[2]Data analysis for capsule 124 is not complete.

The complete representation of the release-rate correlation combines equation (2) with the linear burnup relation (eq. (1)) to give equation (3).

$$r = (1 + 0.49\ b)\left[\frac{dYSLf}{4T} + fYS\left(\frac{D_{fo}f + D_o e^{-Q/RT}}{\lambda}\right)^{1/2}\right] \qquad b > 1.5 \text{ percent} \qquad (3)$$

By analysis of the Kr^{88} release-rate data for capsule 123 (fig. 10), values for the unknown constants in equation (3) were determined. The numerical form of equation (3) is

$$r = (1 + 0.49\ b)\left[\frac{7.4\times10^{-4}fY}{T} + fY\left(\frac{1.7\times10^{-29}f + 5.6\times10^{-8}e^{-156000/RT}}{\lambda}\right)^{1/2}\right] \qquad (4)$$

Values for d and D_{fo} were determined from the lower temperature ($T \leq 1000$ K) release-rate data. Next, the values for D_o and Q were determined from the higher temperature data; D_o and Q (representing atomic diffusion) are unimportant at the lower test temperatures. Equation (4) can be directly compared to the data presented in figure 10 by using the sweep-gas-activity - release-rate expression (eq. (B1) of appendix B)

$$r = \frac{\dot{A}\dot{Q}e^{\lambda V/\dot{Q}}}{\lambda} \qquad (5)$$

The solid lines drawn in figure 14 (which repeats the data in fig. 10) represent the values calculated from the semiempirical equation (4) and equation (5). The calculated lines shown in figure 14 agree closely with the measured data points. The mean deviation is within 11 percent for burnups over 1.5 percent.

When the constants determined from the capsule 123 data are used the calculated release rates are within ±14 percent of the measured values for capsule 121 (fig. 15) and are consistently higher than the measured values for capsule 122 (fig. 16). Data for these two capsules are given in appendix B.

In appendix B it is pointed out that the gas sample activities have an estimated accuracy of ±10 percent, and that the calculated fission-rate densities are accurate to within an estimated ±15 to ±20 percent. Thus, the values found for the constants in equation (3) are no more accurate than these figures.

We can compare the values found for some of the constants in equation (3) with values reported in the literature.

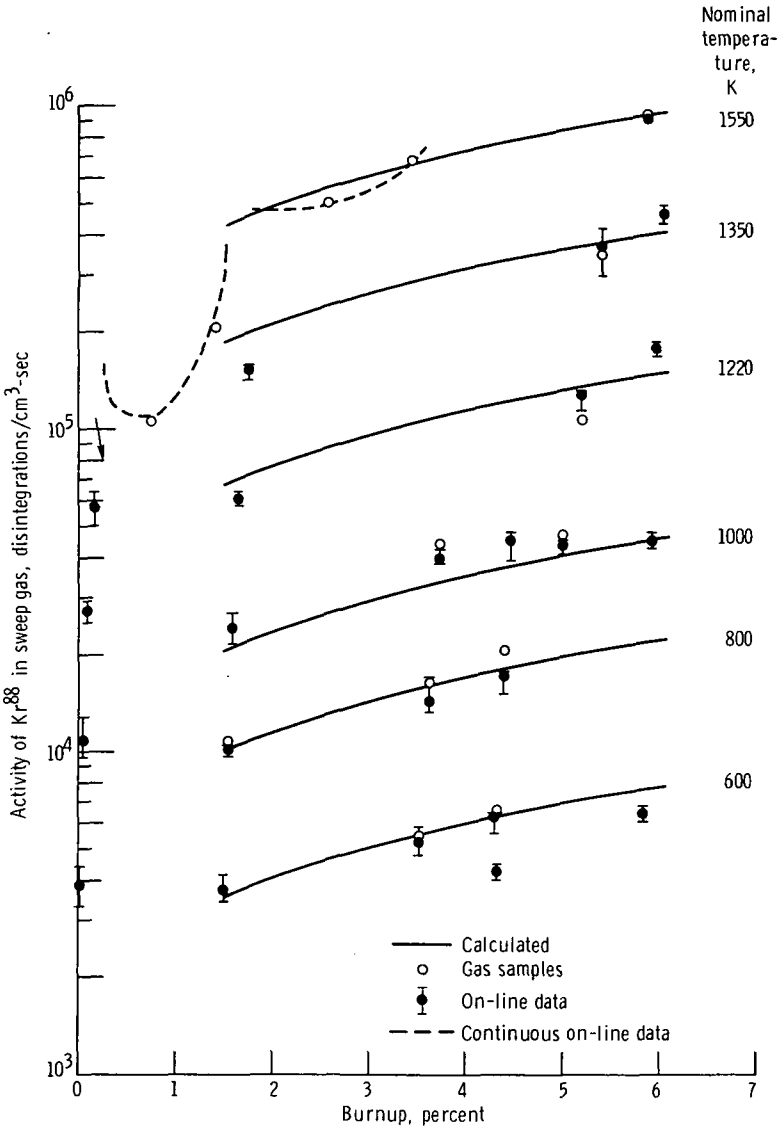

Figure 14. - Comparison of empirical relation with data: activity of krypton-88 as function burnup - capsule 123.

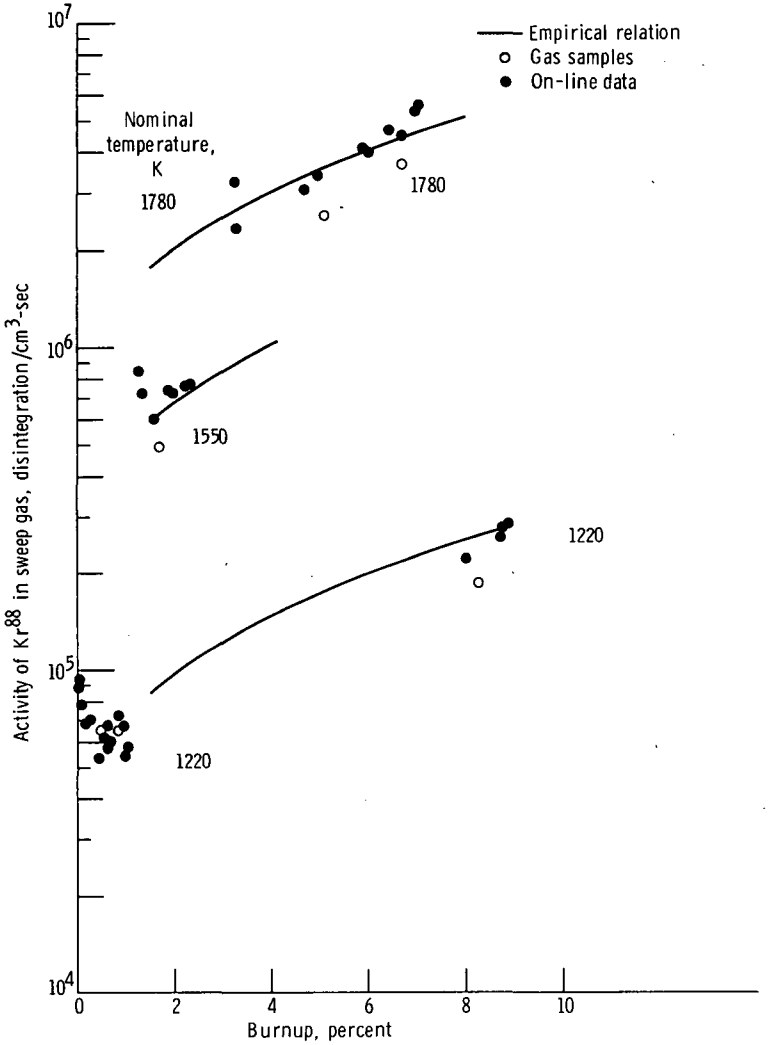

Figure 15. - Comparison of empirical relation with data: activity of krypton-88 as function of burnup - capsule 121.

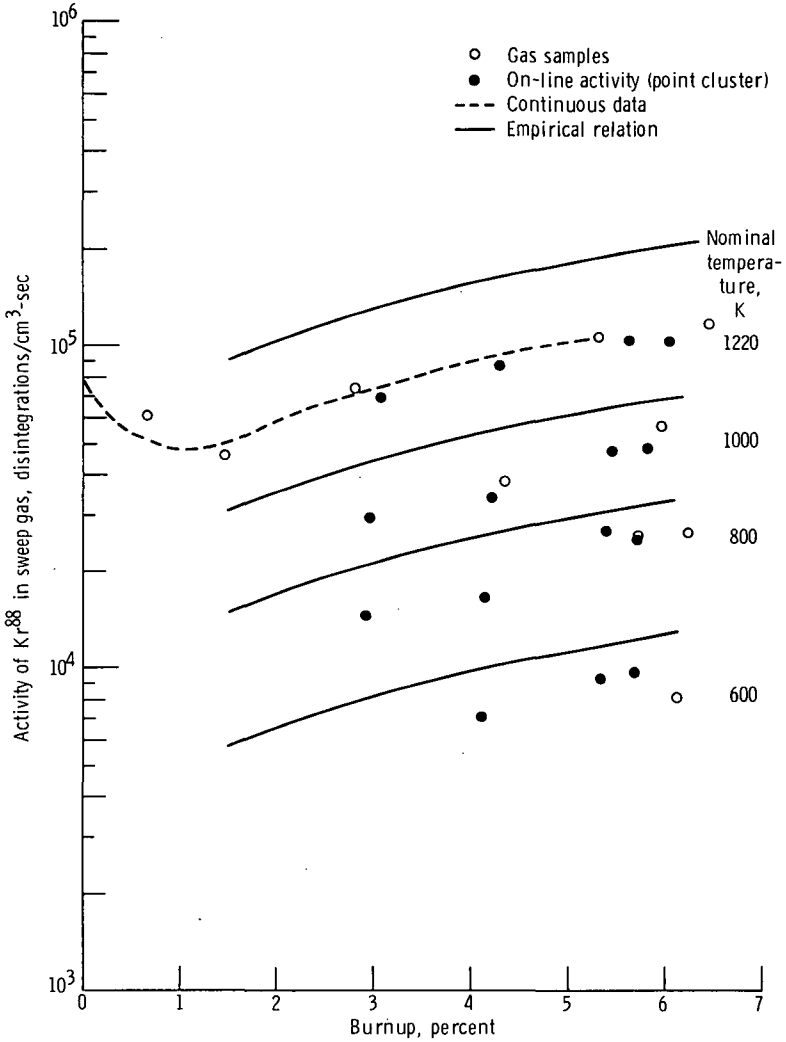

Figure 16. - Comparison of empirical relation with data: activity of krypton-88 as function of burnup - capsule 122.

The value for the group of constants dSL/4 (direct recoil release) which best fits our data is 7.4×10^{-4}. If we use a recoil length in UN of 4.8×10^{-4} centimeter and a geometric surface area of 0.61 square centimeter, the fraction of recoils stopped by the helium at 330 K can be calculated (see appendix C) to be

$$K = 7.4\times10^{-4}\left(\frac{4}{TSL}\right) = 3.1\times10^{-2}$$

Belle (ref. 9) reports that the fraction of recoils that are stopped by a gas gap between fuel and clad is given by

$$K \sim \frac{2h}{l}$$

For our pin, if we use an h of approximately 0.076 centimeter (i.e., the specimen inside diameter) and an l of approximately 2.3 centimeters,[3] $K \sim 2h/l$, or greater than 6.6×10^{-2}. The discrepancy between measured and calculated values for K is not actually a factor of 2. The true gas length traversed by a recoil fragment for our pin would be somewhat less than the 0.076 centimeter used for h.

Brinkman (as reported by Nelson in ref. 1) found that the fission-enhanced self-diffusion coefficient in uranium could be approximated by $D_f \sim 1.5\times10^{-31}f$. Nelson states that this value could represent enhanced gas atom diffusion to within an order of magnitude. We have obtained a value of 1.7×10^{-29} for the combination of terms $D_{fo}S^2$, where S is the surface area of the fuel. Later, in our analysis of total gas release from the fuel, we will show that - after assuming complete interconnection of grain boundary porosity - our value for D_{fo} would be approximately 1.3×10^{-30} cm^2/sec.

Isotopic variation in release rates. - On-line activity measurements for Kr^{85m}, Kr^{87}, and Xe^{135} were made in addition to those reported for Kr^{88}. Analysis of sweep gas samples added data for Xe^{133}. The release rates for all the measured isotopes showed the same increase with burnup as found for Kr^{88}, that is, $r/r_o = (1 + 0.49\ b)$, although the data analysis was not as detailed as for Kr^{88}.

Another important observation is that the relative isotopic release rates do not appreciably shift with changes in temperature and fission-rate density. This is shown in

---

[3]Estimated for helium at 330 K and 6.9×10^5 N/m^2 (100 psia) from measurements in ref. 10 and density-temperature corrections in ref. 11.

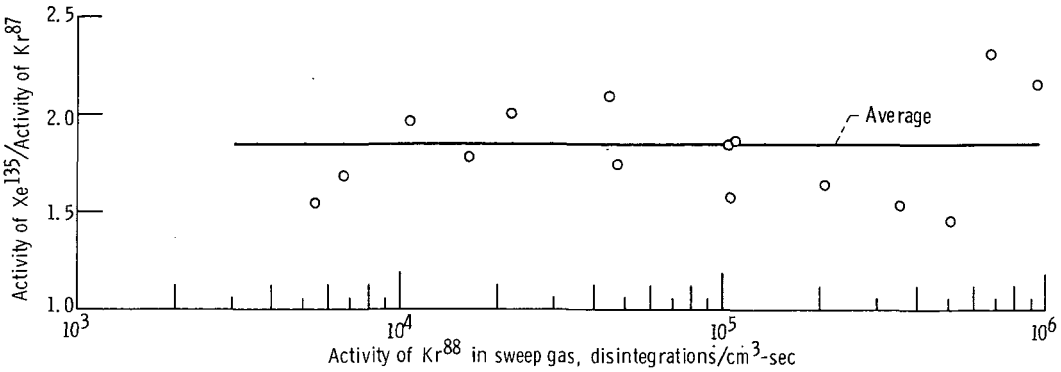

Figure 17. - Isotopic activity ratios as function of krypton-88 activity. Temperature varies from 600 to 1550 K. Decay constant, sec^{-1}: xenon-135, 2.09×10^{-5}; krypton-87, 1.48×10^{-4}.

figure 17 where the activity ratio $A_{Xe^{135}}/A_{Kr^{87}}$ is plotted as a function of krypton-88[4] sweep gas activity, which increases with temperature, fission-rate density, and burnup. This observation seems to imply a single controlling fission-gas transport mechanism.

The isotopic variations in release rates allow us to check equation (3), which predicts an approximate variation of the form $r \propto (1/\lambda)^{1/2}$. Combining this relation with equation (5) for isotopes 1 and 2 gives us the convenient form

$$\frac{A_1}{A_2} = \frac{Y_1}{Y_2}\left(\frac{\lambda_1}{\lambda_2}\right)^{1/2} \frac{e^{-\lambda_1 V/\dot{Q}}}{e^{-\lambda_2 V/\dot{Q}}} \tag{6}$$

In table III we present the calculated and measured activity ratios for various isotope pairs. The results indicate that the variation with decay constant is roughly as predicted by equation (3).

Postirradiation examination results. - Postirradiation fuel microstructures for capsules 123 and 122 are shown in figures 18 to 22. Comparison of figure 20 (capsule 123, x500) and figure 22 (capsule 122, x500) with the preirradiation microstructure (fig. 6) shows that additional porosity has developed. In figure 22 this additional porosity is in the form of relatively few, small, intragranular voids, approximately 0.5 to 1 micrometer in diameter, uniformly dispersed throughout the fuel except near the inside radial surface, where there is a high void density. Figure 20 (capsule 123) shows more and larger (0.5 to 2 μm) intragranular voids preferentially located on the higher temperature side of each grain (side of grain facing right or toward inside surface). Fig-

[4]Krypton-88 activity was chosen for the abscissa in fig. 16 simply because the data analysis for this isotope was the most detailed.

TABLE III. - COMPARISON OF CALCULATED AND MEASURED ISOTOPIC ACTIVITY RATIOS

Isotope pair		Calculated activity ratio, A_1/A_2, if mechanism is -			Measured[a] activity ratio
1	2	$r \propto (1/\lambda)^{1/2}$	$r \propto (1/\lambda)$	$r \neq f(\lambda)$	
Kr^{85m}	Kr^{87}	0.487	0.905	0.262	0.584
Kr^{85m}	Kr^{88}	.331	.418	.262	.371
Kr^{88}	Kr^{87}	1.48	2.17	1.01	1.57
[b]Xe^{135}	Kr^{87}	1.91	5.07	.717	1.85

[a]Average of 17 gas samples for capsule 123.

[b]Neglects neutron absorption in Xe^{135} and iodine decay to xenon outside the fuel.

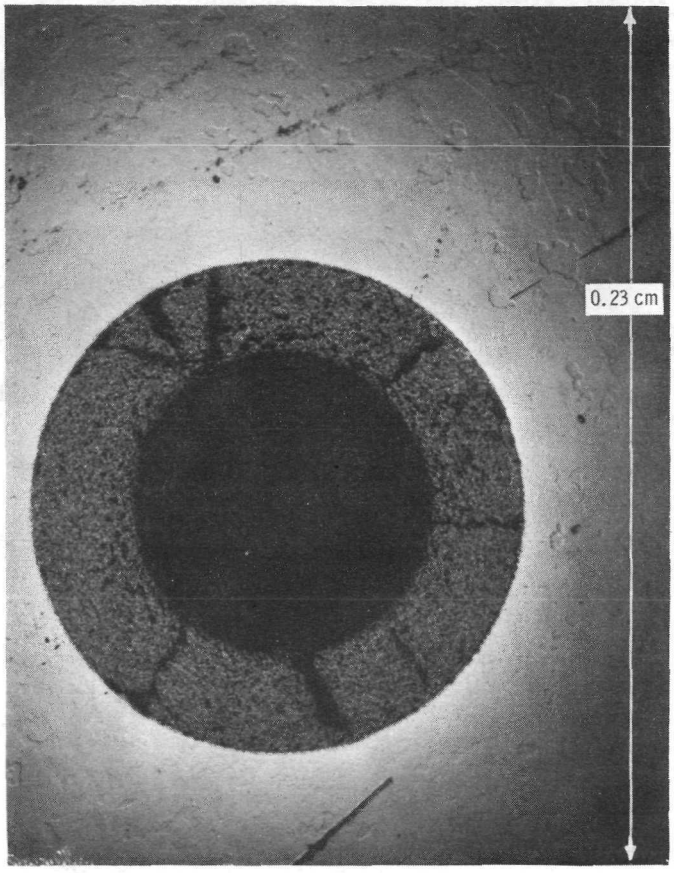

Figure 18. - Section of fuel pin - capsule 123, X50.

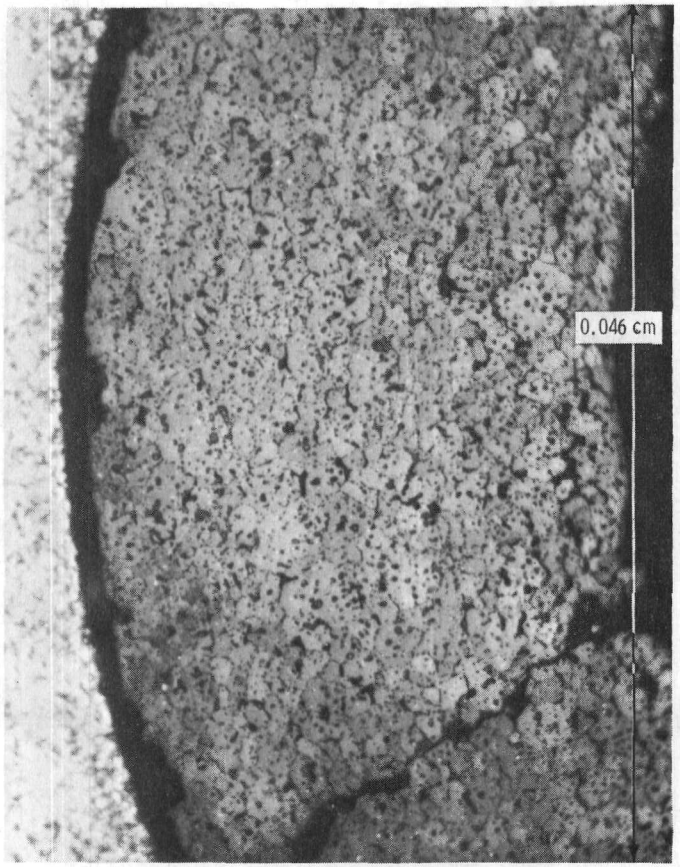

Figure 19. - Section of fuel pin - capsule 123, X250.

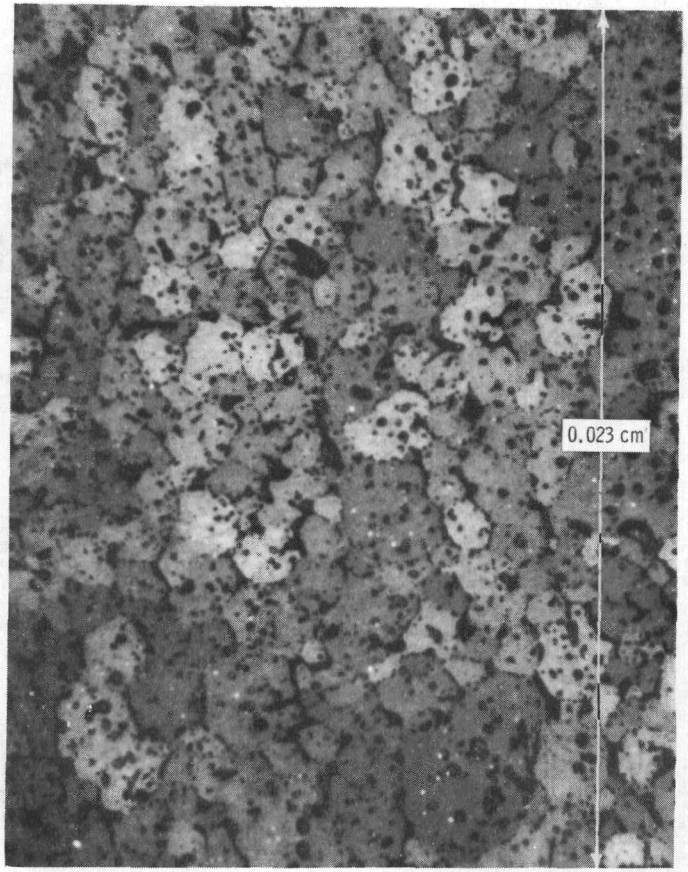

Figure 20. - Section of fuel pin - capsule 123, X500.

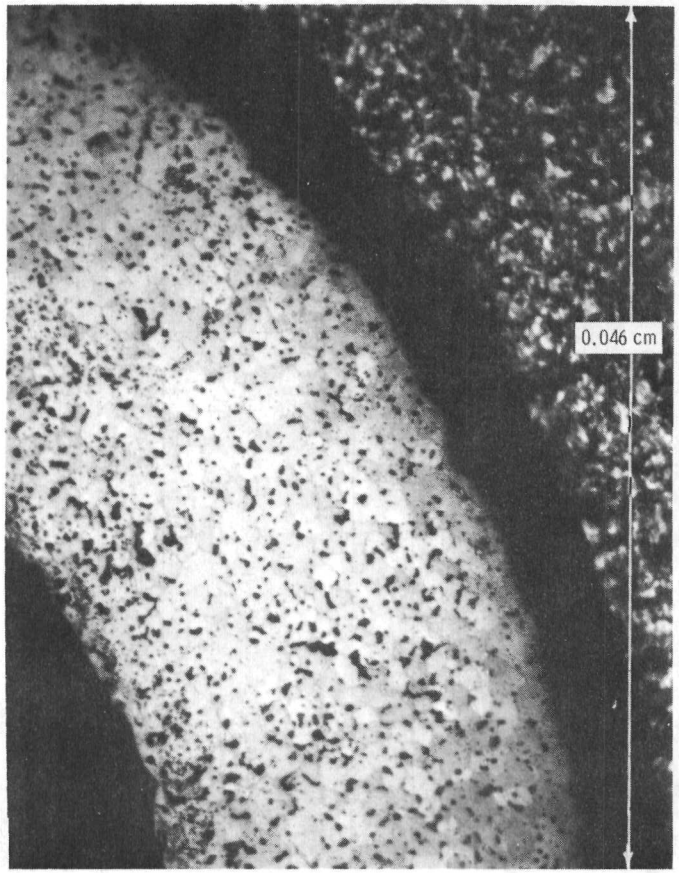

Figure 21. - Section of fuel pin - capsule 122, X250.

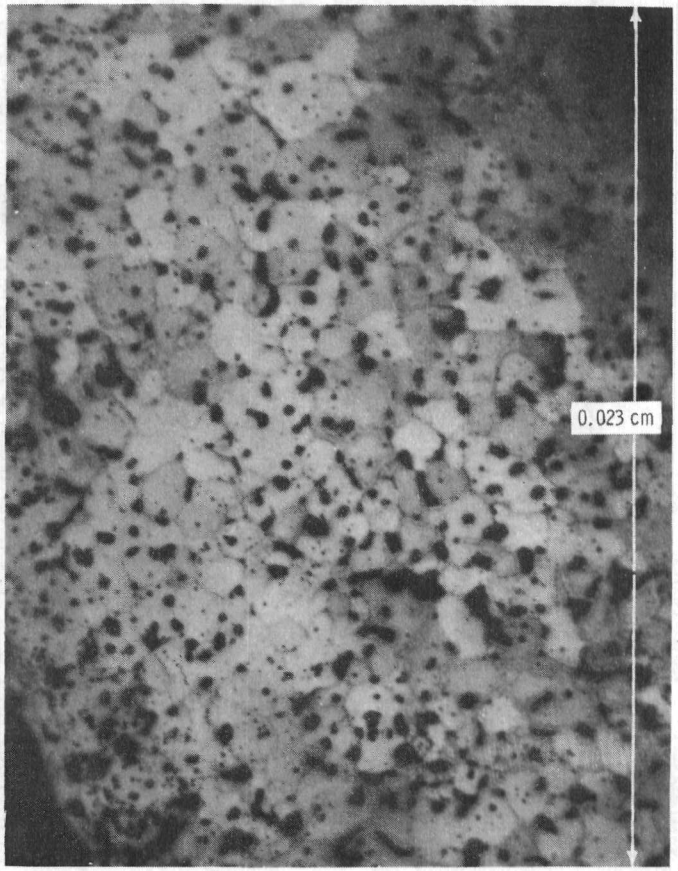

Inside radius

Outside radius

Figure 22. - Section of fuel pin - capsule 122, X500.

ure 20 also shows interconnected intergranular porosity oriented perpendicularly to the direction of the temperature gradient.

Figure 19 (capsule 123, x250) and figure 21 (capsule 122, x250) show the entire fuel thickness for each capsule and reinforce the previous observations about void number, size, and location.

There has been some fuel swelling observed. The specimen swelling in capsule 123 is a representative case and is discussed here. At assembly, the fuel-clad interface gap varied from about 0.6×10^{-3} to 1.0×10^{-3} centimeter. Figure 18 shows the postirradiation interface gap to be less than one-half the original size. The fuel inside diameter does not appear to have changed. The calculated volumetric increase (assuming isotropic fuel swelling) is about 3 to 6 percent. It is quite possible that the fuel was constrained by the heavy walled clad. The small postirradiation interface gap seen in figure 18 is what would be expected had the fuel swelled during irradiation, made contact with the constraining clad, and then separated on cooldown because of the unequal contraction of the two materials.

As mentioned in the section TEST PROCEDURES, the postirradiation examinations include measurements to determine vented uranium and gross fission product retention and release (as indicated by Cs^{137}). Results for the three irradiations are presented in table IV.

The boiling point of cesium (943 K) indicates that cesium should have been gaseous during all our tests. Thus, it should be possible to calculate the long-lived cesium release by extending our model to include stable gases.

TABLE IV. - FUEL AND FISSION PRODUCT LOSS FROM FUEL SPECIMENS

	Capsule 121	Capsule 122	Capsule 123
Primary test temperature, K	1780	1220	1550
Vented uranium[a] (in nitric acid leach solution), mg	0.3	<0.2 (not detected)	-----
Average Cs^{137} retained, percent	22	99[b]	55[c]
Cs^{137} lost (in leach solution), percent	65	3.4	40.5[d]
Average Ce^{141} retained, percent	93	96	-----
Ce^{141} lost (in leach solution), percent	0.2	<1	<0.1

[a]Initial fuel weight for each capsule was ~0.24 g.

[b]A second sample showed 185-percent retention.

[c]A third sample showed 15-percent retention.

[d]Efficiency of nitric acid leach not known; Cs^{137} losses are at least as high as given.

Equation (7) (which was derived as eq. (D26) in appendix D) gives the total stable gas release-birth ratio

$$\frac{r_T}{B} = \frac{KL}{4y_2} + 1 - \frac{8}{\pi^2} \sum_{n=0}^{\infty} \frac{1 - e^{-(2n+1)^2 \alpha}}{(2n+1)^4 \alpha} \tag{7}$$

where

$$\alpha \triangleq (D_f + D)\pi^2 \frac{t}{4y_2^2}$$

Before this equation can be used to calculate r_T/B, we must obtain an estimate of the total surface area at the end of the irradiation period. The constants previously determined in order to fit equation (3) to the radioactive-gas release rate data include combinations of terms like $D_{fo}S^2$ and D_oS^2, where S and D_o are not separable.

If we assume complete interconnection of the grain boundary porosity in the circumferential direction, the true surface area is approximately 14 square centimeters; and the correct length to use in equation (7) is the half-grain thickness ($\sim 7.5 \times 10^{-4}$ cm).

Calculated Cs^{137} releases for capsules 121, 122, and 123 are compared to the measured releases in table V. The calculated releases do not include recoils (<1 per-

TABLE V. - COMPARISON OF CALCULATED AND MEASURED CESIUM-137 RELEASES

Capsule	Temperature, K	Time, t, hr	Release parameter, α	Ratio of total release to birth, r_T/B	
				Calculated	Measured
121	1785	460	0.859		
	1780	80	.089		
	1550	170	.066		
	1225	585	.013		
			$\sum\alpha = 1.027$	0.48	0.65 to 0.78
122	*1225*	*1375*	*0.0315*	*0.085*	*0.01 to 0.03*
123	1540	680	0.242		
	1385	180	.017		
	1225	215	.004		
			$\sum\alpha = 0.263$	0.25	0.40 to 0.45

cent) nor any additional burst releases caused by abrupt temperature changes.

The discrepancy between the measured and calculated total Cs^{137} release for capsule 122 was expected since figure 22 does not show the large-scale interconnection of grain boundary porosity of the fuel in capsule 123 (fig. 20).

While this analysis is very approximate in nature, it does indicate that the large fission-gas releases measured in these tests can be best explained by combining releases from individual grains with a gross interconnection of grain boundary porosity.

Discussion

Based on a simple recoil, atomic-diffusion, fission-enhanced-diffusion model, a fission-gas release-rate equation (eq. (3)) was derived and used to correlate the steady-state fission-gas release-rate data obtained with the sweep gas facility. Constants in the release-rate equation were determined from the test data taken with capsule 123 (fig. 10 or 14), so that for this capsule the mean deviation is within 11 percent (for burnups over 1.5 percent). When the same constants are used, the calculated release rates are within ±14 percent of the measured values for capsule 121 and are consistently higher than the measured values for capsule 122.

Both capsules 121 and 123 were irradiated to high fission burnups (8.3 percent and 6.0 percent, respectively) at temperatures over 1500 K. Capsule 122 was irradiated at a maximum temperature of 1225 K. As is shown by postirradiation photomicrographs (figs. 20 and 22), the UN irradiated in capsule 123 (fig. 20) contains large, 0.5 to 2 μm, gas bubbles plus interconnected grain boundary porosity, while the UN irradiated in capsule 122 (fig. 22) contains smaller bubbles with little or no grain boundary porosity.

The gas transport-release model can also be extended to explain the high release of Cs^{137} from the fuel if it is assumed that the fission gas is released first to the grain boundaries and then from the fuel. The presence of interconnected grain boundary porosity in the photomicrographs of the fuel in capsule 123 (figs. 18 to 20) supports this view.

Recently reported gas release data for $(U_{0.8}Pu_{0.2})N$ irradiations (ref. 12) has been interpreted as being related to surface-connected porosity. This interpretation has also been used to explain data obtained in UN irradiations (ref. 12).

The $(U_{0.8}Pu_{0.2})N$ data reported in reference 12 show a steep increase in gas release at about 1-percent burnup. At this point, pore interconnection is taking place. Test data for Kr^{88} release at 1550 K for capsule 123 (fig. 10) show a large increase at about 1-percent burnup - at which point, pore interconnection may be taking place.

Our gas transport-release model does not include a description of directed bubble migration. Evidence for the existence of this mechanism was presented in figures 20

and 22. Consideration of this process as one which contributes to fission-gas release is consistent with our data.

Analysis of high-temperature-gas release rates shows the exponential temperature dependence ($e^{-Q/RT}$ in eq. (2)), which we assumed to be caused by gas diffusion in the fuel. Nichols (ref. 4) shows that pore migration up a temperature gradient is dependent on temperature in approximately the same manner if the controlling mechanism is surface diffusion, volume diffusion, or evaporation-condensation.

The UN fuel specimens irradiated in this program were operated with large (for UN) temperature gradients of as much as 500 K/cm. These gradients are a driving force for pore migration.

A dynamic gas resolution process may also be important in describing fission-gas transport through the fuel. Gas permanently trapped in bubbles moving up a thermal gradient would be expected to attain a concentration varying approximately as $1/\lambda$. If no interchange existed between the gas held in the pores and the gas diffusing through the fuel, we could expect to observe a definite shift in relative isotopic release rates as the fuel temperature increased and the release controlling mechanism changed from atomic-plus-fission-enhanced diffusion to bubble diffusion.

Our results, such as those shown in figure 17, indicate no shift in relative isotopic release rates when the fuel temperature changes from $\sim$800 K to 1550 K.

This view of fission-gas transport in the fuel is consistent with ideas presented in many recent papers. For example, Carroll, in his review article (ref. 2), concludes that fission gas is in "constant turmoil" within fissioning fuel specimens. Gas resolution and pore migration mechanisms can both be important in explaining fission-gas transport within fissioning fuel.

We have noted that the high thermal gradients present in our fuel specimens would act as a driving force for pore migration. Similarly, our high fission-rate densities would increase the rate of gas resolution.

The preliminary fission-gas transport-release model utilized in this report to predict the total Cs^{137} releases from high-burnup (>6 percent), high-temperature (>1500 K) UN specimens should not be directly applied to UN fuel pins operating at low-burnup and/or low-temperature conditions. A basic assumption in our utilization of equation (7) to calculate Cs^{137} releases was that all the fission gas released from individual UN fuel grains was ultimately released from the specimen. Photomicrographs of specimen 123 operated to 6-percent burnup at 1505 K (figs. 19 and 20) show the presence of interconnected intergranular porosity. Gas released from individual grains can easily get to the exterior fuel surface. Without the formation of interconnected porosity, gas released to interior grain boundaries may be trapped and not released from the fuel pin.

It is possible that low-burnup, low-temperature, fission-gas release can be de-

scribed by using our equations (such as eq. (7)) but considering only those grains which touch the geometric surface of the fuel. As the fuel burnup increases, more gas is released to the grain boundaries and finally some or all of this gas can escape through interconnected intergranular porosity.

SUMMARY OF RESULTS

This section contains a basic summary of experimental fission-gas release results obtained from small uranium nitride specimens irradiated to 8-percent burnup at high fission-rate densities:

1. Release rates of the three krypton isotopes examined (Kr^{85m}, Kr^{87}, and Kr^{88}) decreased with increasing burnup during the low-burnup (0 to 1 percent) period of our irradiation tests. This decrease was observed at fuel temperatures from 800 to 1500 K.

2. After a fuel burnup of approximately 1.5 percent, fission-gas release rates increased linearly with burnup, independent of test history, to over 8-percent burnup (upper test limit).

3. Postirradiation photographs of the capsule 123 fuel microstructure show grain boundary porosity oriented perpendicularly to the direction of the temperature gradient, as well as intragranular porosity preferentially located on the higher temperature side of each grain.

4. The release rates of one isotope relative to another did not change appreciably with any test conditions.

5. The variation of krypton release rate r with fission-rate density, temperature, and total burnup ($b > 1.5$ percent) for capsules 121 and 123 can be described by

$$r = (1 + 0.49\,b)\left[\frac{7.4\times10^{-4}fY}{T} + fY\left(\frac{1.7\times10^{-29}f + 5.6\times10^{-8}e^{-156000/RT}}{\lambda}\right)^{1/2}\right]$$

where f is fission-rate density, Y is fractional fission yield, T is temperature, R is the gas constant, and λ is the decay constant.

Lewis Research Center,
National Aeronautics and Space Administration,
Cleveland, Ohio, November 7, 1972,
503-05.

APPENDIX A

NUCLEAR ENVIRONMENT

In order to more fully characterize the fuel specimen test conditions, the nuclear environment for each of the three specimens is outlined in table VI. The tabulated

TABLE VI. - NUCLEAR ENVIRONMENT FOR SPECIMENS

Capsule	Maximum thermal neutron flux in fuel, neutrons/cm^2-sec	Maximum gamma heating rate in fuel, W/g	Thermal neutron fluence, neutrons/cm^2	Fast neutron fluence (>0.1 MeV), neutrons/cm^2
121	5×10^{13}	3	2×10^{20}	10^{19}
122	2	2	1	10^{19}
123	3	3	1	(Not measured)

thermal-neutron-flux and gamma-heating-rate information is based on the specimen location in the reactor test hole during irradiation (with corrections applied depending on the reactor operating power and control rod bank height). Support tests were performed in the Plum Brook Mockup Reactor to determine the neutron-flux and gamma-heating-rate profiles along the length of the reactor test hole. A dummy capsule was used to obtain the information required to establish the capsule-specimen flux perturbation factors.

Each test specimen was subjected to several thermal flux levels in order to achieve the fission heat generation rates required to maintain the several desired test temperatures. The tabulated values for thermal flux and gamma heating rate are the highest to which each specimen was subjected.

The tabulated thermal and fast neutron fluence values were determined through the analysis of dosimeter wires located within and at the outside surface of each capsule. Aluminum-cobalt wires were used for determining the thermal fluence. Nickel and stainless-steel (300 series) wires were used for the fast fluence determinations. The thermal fluence dosimeters were located an appreciable distance from the fuel specimen. Hence, corrections were applied to the measured values in order to determine the appropriate thermal fluence values for the fuel specimens. The required correction factors were determined in the Mockup Reactor tests.

APPENDIX B

DATA AND DATA REDUCTION

Of the variables of interest (release rate, temperature, fission-rate density, and burnup) only one, the temperature, was obtained from direct measurements. Fission-gas release rates were calculated from measured activities in the sweep gas, either from samples counted by the Plum Brook Radiochemistry Section or from on-line scintillation detector data. Absolute fission-rate densities were calculated from measurements of relative thermal flux as a function of position in test hole (relative fission-rate densities) combined with the total burnup obtained in the postirradiation examinations. Burnup could be calculated at any time during the irradiation by knowing total burnup and test history.

An understanding of the accuracy to which the variables are known can be obtained by following through the sequence of steps in the data reduction procedure, as is done in this section.

Sweep Gas Activities and Fission-Gas Release Rates

Fission-gas activities in the helium sweep gas were determined by gamma-ray counting techniques, by using either an on-line scintillation detector or a Ge(Li) detector for the gas samples. Analysis of the gas samples was estimated to give activities accurate to ±10 percent for the isotopes Kr^{85m}, Kr^{87}, Kr^{88}, and Xe^{135}. An unknown error is introduced here; literature values for absolute gamma-ray intensities (gammas of a particular energy per disintegration) must be used. The values used are shown in table VII, and particular note of the range of values reported for Kr^{87} should be made.

TABLE VII. - GAMMA-RAY INTENTISY DATA

Isotope	Gamma-ray energy, MeV	Gammas per 100 disintegrations	Reference
Kr^{85m}	0.150	75.2	13
Kr^{87}	.403	[a]59.6	14
		50	15
		~68	16
Kr^{88}	2.392	37.8	17
Xe^{135}	.250	97	18

[a]Value used in data analysis.

TABLE VIII. - FISSION-GAS ACTIVITY IN HELIUM SWEEP GAS - CAPSULE 121 GAS SAMPLES[a]

Fuel maximum temperature, K	Fission-rate density, fissions/cm^3-sec	Fuel burnup, percent	Isotope activity, disintegrations per cm^3 per second			
			Kr^{85m}	Kr^{87}	Kr^{88}	Xe^{135}
1236	3.43×10^{14}	0.54	30.2×10^3	55.9×10^3	63.4×10^3	69.8×10^3
1240	3.47	.82	29.7	52.7	59.7	64.5
1550	5.77	1.7	262	398	490	726
1765	7.97	5.06	1320	1780	2560	3650
1765	7.97	6.65	2100	2280	3690	5810
1215	3.30	8.3	95.9	184	183	227

[a]Some samples obtained during each capsule test grossly disagreed with on-line data, probably because of leaks or incomplete filling. These have not been tabulated.

TABLE IX. - FISSION-GAS ACTIVITY IN HELIUM SWEEP GAS - CAPSULE 122 GAS SAMPLES

Fuel maximum temperature, K	Fission-rate density, fissions/cm^3-sec	Fuel burnup, percent	Isotope activity, disintegrations per cm^3 per second			
			Kr^{85m}	Kr^{87}	Kr^{88}	Xe^{135}
1222	3.64×10^{14}	0.49	24.1×10^3	38.8×10^3	60.5×10^3	50.1×10^3
1209	3.43	1.48	20.5	33.3	45.5	45.3
1223	3.64	2.64	30.6	50.7	73.5	68.3
1000	2.33	4.31	15.8	24.5	38.5	41.2
1225	3.64	5.38	40.3	65.5	104	106
800	1.44	5.81	8.34	15.9	25.7	25.2
1000	2.33	5.93	22.4	35.3	57.2	58
598	.71	6.16	3.20	5.35	8.00	8.04
805	1.45	6.27	10.1	16.5	26.1	26.3
1227	3.64	6.59	44.3	71.2	118	121

The fission-gas activities in the sweep gas as determined from gas samples for each of the three specimens tested are presented in tables VIII to X along with other pertinent test data. A discussion of how we obtained the values for fission-rate density is presented later in this appendix.

A typical scintillation detector spectrum is shown in figure 23. Integration under the peaks corresponding to the different isotopes yielded relative activities which could be converted to absolute activities by comparison with gas samples. Activities determined by each method are compared in table XI.

On-line activity data for each of the capsules are plotted as a function of burnup in

TABLE X. - FISSION-GAS ACTIVITY IN HELIUM SWEEP GAS -

CAPSULE 123 GAS SAMPLES

Fuel maximum temperature, K	Fission-rate density, fissions/cm^3-sec	Fuel burnup, percent	Isotope activity, disintegrations per cm^3 per second			
			Kr^{85m}	Kr^{87}	Kr^{88}	Xe^{135}
1540	4.47×10^{14}	0.75	41.1×10^3	71×10^3	104×10^3	131×10^3
1536	4.46	1.42	79.7	144	206	237
800	1.09	1.54	4.36	6.79	10.7	13.3
1534	4.45	2.59	185	326	504	556
1543	4.49	3.45	256	426	685	993
580	.48	3.52	1.84	3.85	5.50	5.97
801	1.09	3.63	6.20	10.8	16.4	19.1
992	1.77	3.72	16.8	26.6	44.1	55.3
591	.50	4.33	2.49	4.85	6.68	8.14
812	1.12	4.39	8.24	13.2	22.0	26.4
1145	2.43	4.88	39.9	67.7	109	127
995	1.78	5.04	17.6	29.8	46.8	51.5
1214	2.75	5.19	36.9	65.7	108	103
1382	3.61	5.39	122	240	351	369
1540	4.47	5.86	357	555	939	1200

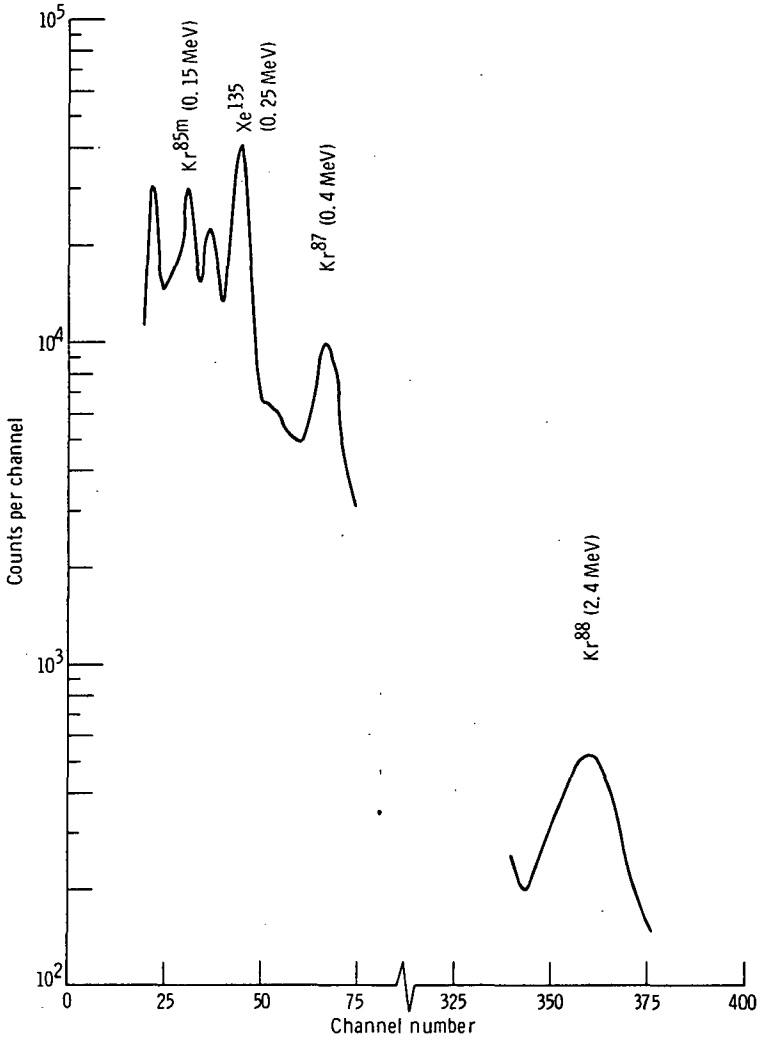

Figure 23. - Representative fission-gas gamma-ray energy spectrum.

TABLE XI. - Kr^{88} ACTIVITY: ON-LINE COUNT RATE COMPARED TO ACTIVITIES MEASURED IN GAS SAMPLES

[Data for capsule 123.]

Sample[a]	Reported activity, disintegrations/cm^3-sec	On-line count rate at 10 cm, counts/sec
1	1.04×10^5	110
2	2.06	250
3	1.07×10^4	9.65
4	5.04×10^5	570
5	6.85	700
6	5.50×10^3	5.35
7	1.64×10^4	14.8
8	4.41	35.0
10	6.68×10^3	5.0
11	2.20×10^4	17.0
13	1.09×10^5	89
15	4.68×10^4	42.0
16	1.08×10^5	130
17	3.51	350
18	9.39	950

Average ratio, $\frac{\text{On-line count rate}}{\text{Sample activity}} = 9.62\times10^{-4}$

Mean deviation from average ratio = ±12 percent

[a]Unused samples show gross disagreement, probably because of leaks.

figures 24 and 25. Nominal temperature is a parameter. Gas sample points have also been included.

Sweep gas activities were converted to release rates by using the equation

$$r = \frac{A\dot{Q}e^{\lambda V/\dot{Q}}}{\lambda} \tag{B1}$$

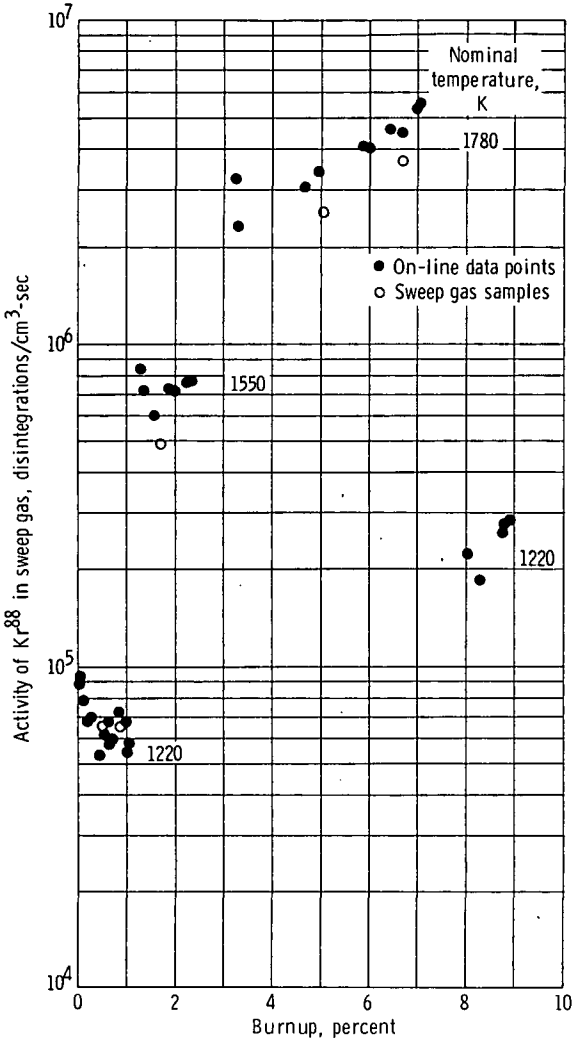

Figure 24. - Activity of krypton-88 as function of burnup - capsule 121.

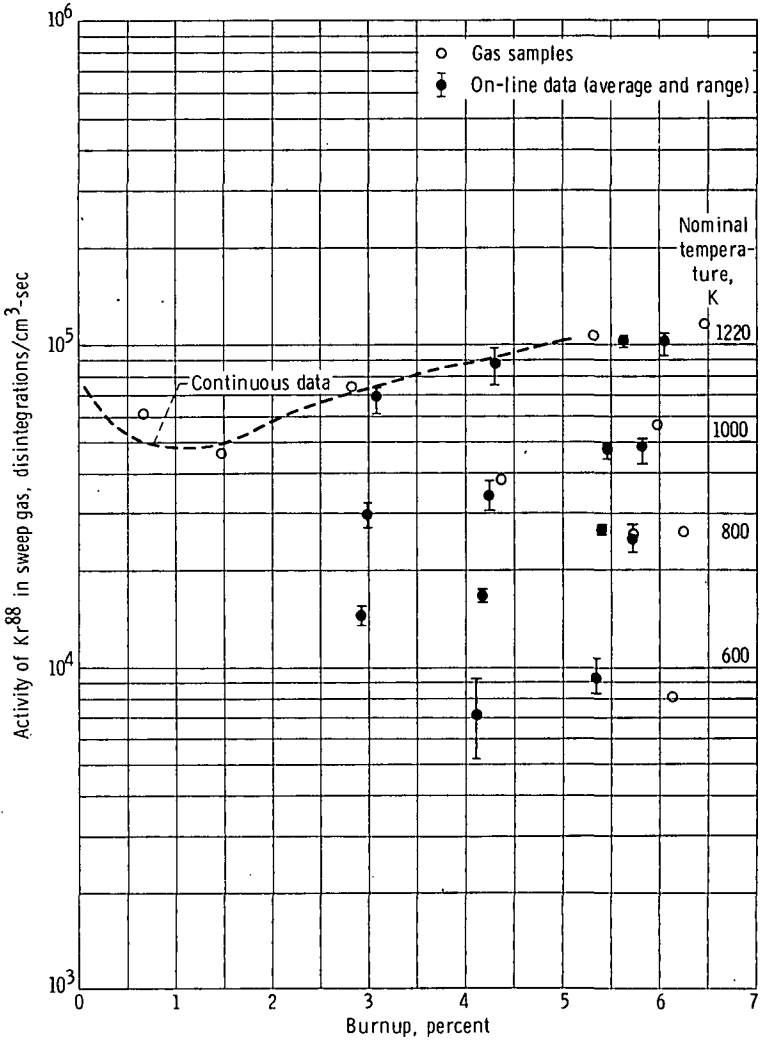

Figure 25. - Activity of krypton-88 as function of burnup - capsule 122.

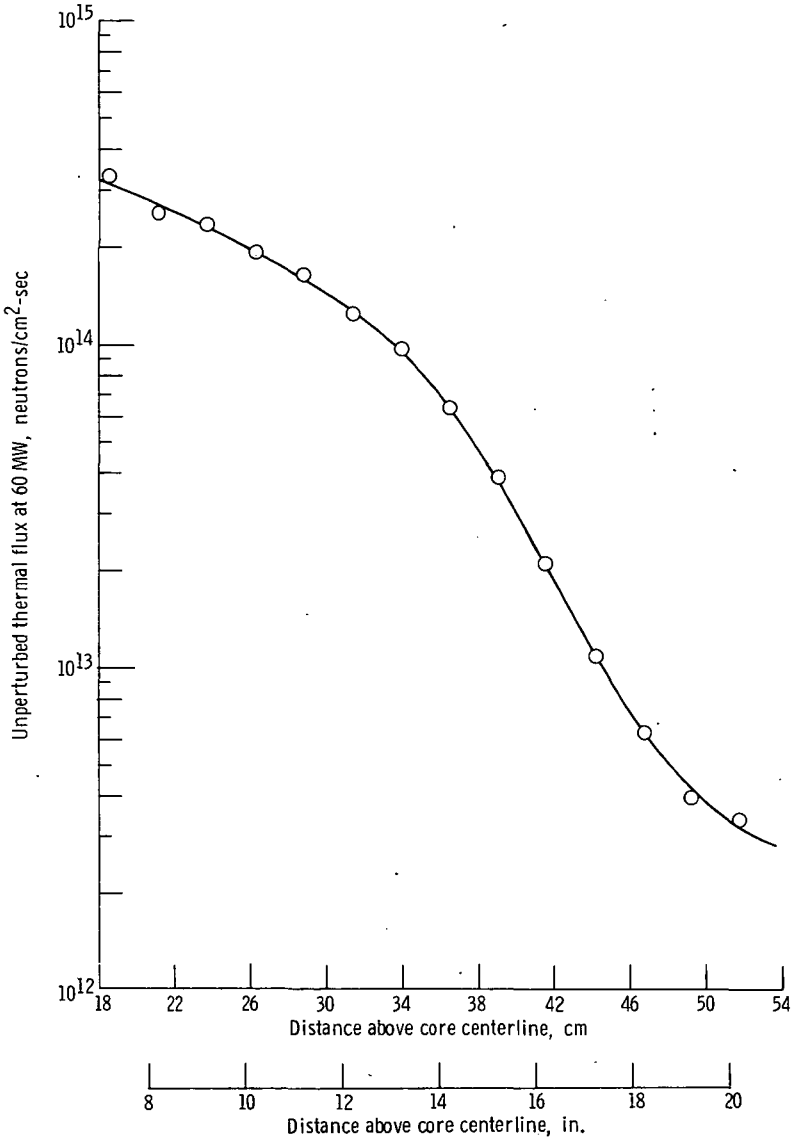

Figure 26. - Unperturbed thermal neutron flux in Plum Brook Reactor test hole RA-5. Values based on Mockup Reactor measurements with rod bank height of 40.51 centimeters (15.95 in.).

Absolute Fission-Rate Densities

Absolute fission-rate densities corresponding to particular fuel-pin temperatures and capsule positions in the Plum Brook Reactor test hole RA-5 were calculated by combining estimates of relative thermal flux (assumed proportional to relative fission-rate density) with postirradiation measurements of total burnup.

For particular capsule test positions we calculated the relative thermal flux by using the thermal flux profile obtained through Mockup Reactor[5] measurements (fig. 26) and corrections for reactor shim-rod position and total power level. Plots of temperature as a function of relative fission-rate density were then prepared for each reactor cycle by assuming that relative fission-rate density equaled relative thermal flux. Cycle-to-cycle variations in reactor characteristics caused by changes in core loading or experiments were eliminated by equating the relative fission-rate densities at one particular temperature. Figure 27 shows a plot of temperature as a function of fission-rate density for capsule 123. For each irradiation cycle, the relative fission-rate density at 975 K was set to unity.

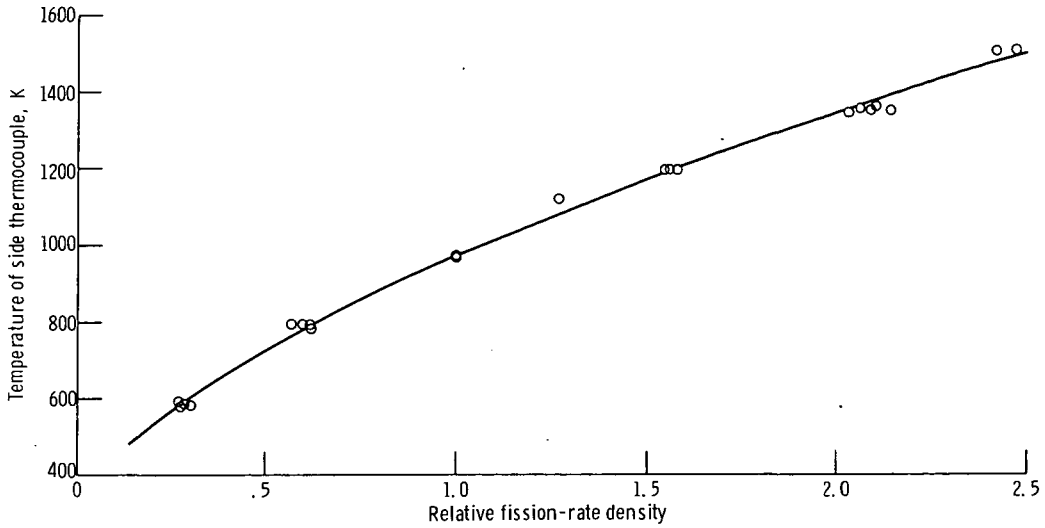

Figure 27. - Temperature as function of relative fission-rate density with each cycle separate - capsule 123.

[5]This Mockup Reactor closely simulates the characteristics of the Plum Brook Reactor (PBR).

Absolute fission-rate densities were obtained by integrating the relative fission-rate densities over each pin's irradiation history and then utilizing the measured total burnup (fissions/cm^3) to get the necessary conversion factors. Figure 28 shows the relation between temperature and fission-rate density for all three capsules.

We have made no corrections for variations in fuel content during irradiation. For all our tests, any corrections would be only a few percent, or much less than the uncertainties inherent in this calculational procedure (15 to 20 percent).

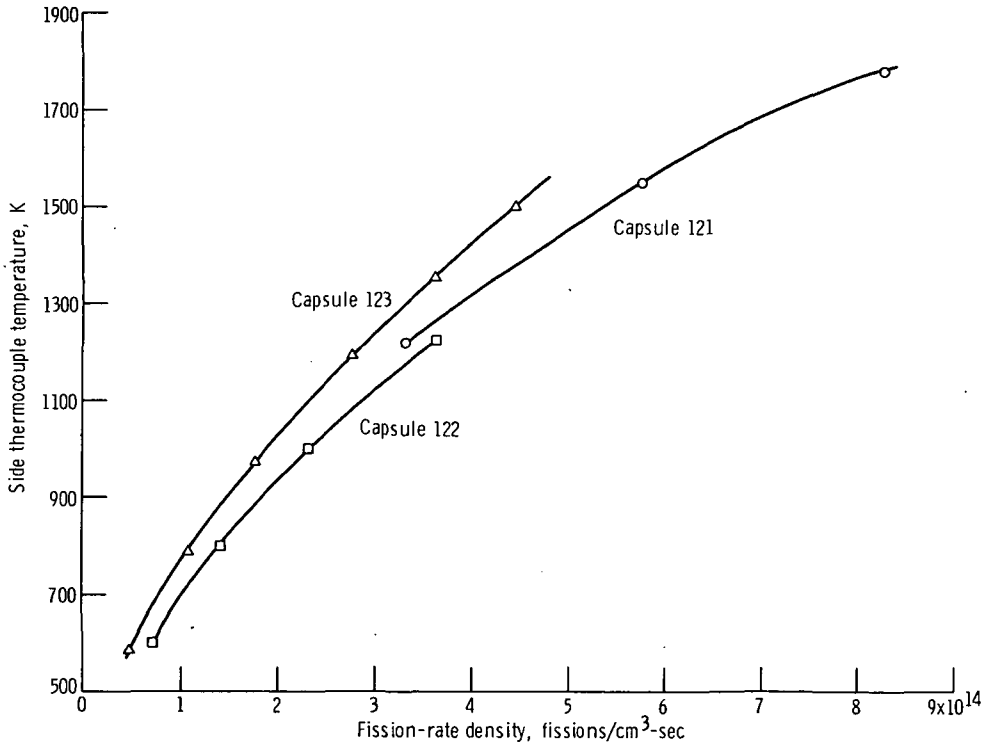

Figure 28. - Temperature as function of fission-rate density - all three capsules.

APPENDIX C

STEADY-STATE FISSION-GAS RELEASE RATE

The general time-dependent equation for diffusional transport of fission gas in a one-dimensional rectangular coordinate system is

$$\frac{\partial c}{\partial t} = (D_f + D)\frac{\partial^2 c}{\partial y^2} - \lambda c + fY \qquad \text{(C1)}$$

where it has been assumed that the diffusion coefficients D_f and D are constants and that the fission-rate density f is independent of position in the fuel.

The steady-state form of equation (C1) is obtained by setting

$$\frac{\partial c}{\partial t} = 0 \qquad \text{(C2)}$$

And the two boundary conditions required to get a complete solution to the steady-state equation are

$$\frac{dc}{dy} = 0 \quad \text{at} \quad y = 0 \qquad \text{(C3)}$$

and

$$c = 0 \quad \text{at} \quad y = y_1$$

where y_1 is the distance across the fuel (fuel thickness).

Descriptively, $dc/dy = 0$ at $y = 0$ represents a barrier to fission-gas transport, such as the fuel clad interface; and $c = 0$ at $y = y_1$ represents the conditions at the fuel-gas interface.

The steady-state solution to equation (C1) with the boundary conditions (C3) is

$$c(y) = \frac{F}{E}\left(1 - \frac{e^{\sqrt{E}\,y} + e^{-\sqrt{E}\,y}}{e^{\sqrt{E}\,y_1} + e^{-\sqrt{E}\,y_1}}\right) \qquad \text{(C4)}$$

where F and E are defined as

$$F \triangleq \frac{fY}{D_f + D}$$

$$E \triangleq \frac{\lambda}{D_f + D}$$

Now we assume that at the fuel surface ($y = y_1$) fission-gas release is given by a recoil component added to the diffusional release. The release equation is

$$r = \frac{KYSLf}{4} - (D_f + D)S \left.\frac{dc}{dy}\right|_{y_1} \tag{C5}$$

where we have assumed that one-fourth of the recoil fragments originating within a distance L of the surface leave the fuel. Combining equations (C4) and (C5) with the simplification

$$e^{\sqrt{E}\, y_1} >> e^{-\sqrt{E}\, y_1}$$

gives

$$r = \frac{KYSLf}{4} + fYS\left(\frac{D_f + D}{\lambda}\right)^{1/2} \tag{C6}$$

D_f can be put into the form (ref. 1)

$$D_f = D_{fo} f$$

where D_{fo} is a constant. D is usually presented as

$$D = D_o e^{-Q/RT}$$

With these relations, equation (C6) becomes

$$r = \frac{KYSLf}{4} + fYS\left(\frac{D_{fo} f + D_o e^{-Q/RT}}{\lambda}\right)^{1/2} \tag{C7}$$

The constant K in equation (C7) is approximately proportional to the density of the gas into which the recoils are ejected (ref. 9, p. 652). Therefore, to describe the change in gas density with temperature, we can replace K by the term d/T, where d is a constant, to give the final form of the steady-state release-rate equation

$$r = \frac{dYSLf}{4T} + fYS\left(\frac{D_{fo}f + D_o e^{-Q/RT}}{\lambda}\right)^{1/2} \qquad \text{(C8)}$$

APPENDIX D

TIME-DEPENDENT STABLE GAS RELEASE

The starting point for this derivation is the one-dimensional transport equation (C1)

$$\frac{\partial c}{\partial t} = (D_f + D)\frac{\partial^2 c}{\partial y^2} - \lambda c + fY \tag{C1}$$

which for a stable gas ($\lambda = 0$) becomes

$$\frac{\partial c}{\partial t} = (D_f + D)\frac{\partial^2 c}{\partial y^2} + fY \tag{D1}$$

Carslaw and Jaeger (ref. 19, pp. 29-30) state that the solution to an equation of this type with initial and boundary conditions

$$\left.\begin{aligned} c(y, 0) &= M(y) \\ c(\text{surface}) &= N(y_2) \end{aligned}\right\} \tag{D2}$$

can be expressed as

$$c(y, t) = u(y) + w(y, t) \tag{D3}$$

where the functions u and w are themselves solutions for

$$\frac{\partial^2 u}{\partial y^2} = \frac{-fY}{D_f + D} \tag{D4}$$

and

$$\frac{\partial^2 w}{\partial y^2} - \frac{1}{D_f + D}\frac{\partial w}{\partial t} = 0 \tag{D5}$$

with initial and boundary conditions

$$\left.\begin{aligned} u(\text{surface}) &= N(y) \\ w(y, 0) &= M(y) - u \\ w(\text{surface}) &= 0 \end{aligned}\right\} \tag{D6}$$

We will first derive the solution for $c(y,t)$ with an arbitrary initial concentration $M(y)$ and boundary conditions

$$\left.\begin{aligned} c(\text{surface}) = c(y_2) &= 0 = N(y_2) \\ \frac{\partial c}{\partial y} &= 0 \quad \text{at } y = 0 \end{aligned}\right\} \tag{D7}$$

Then this solution will be specialized to the cases

$$M(y) = 0 \tag{D8}$$

(zero initial concentration) and

$$M(y) = c(y, \tau) \tag{D9}$$

where $c(y, \tau)$ is the concentration found by using condition (D8) for a specific set of constants D_f, D, and f at time τ. Equations for stable gas release rates can be obtained for the special cases.

Arbitrary Initial Concentration

As given by equation (D3), the concentration c is

$$c(y,t) = u(y) + w(y,t) \tag{D3}$$

where $u(y)$, as defined by equation (D4) with boundary condition (D7), has the solution

$$u(y) = \frac{fY}{2(D_f + D)}\left(y_2^2 - y^2\right) \tag{D10}$$

Then $w(y,t)$ is the solution to equation (D5)

$$\frac{\partial^2 w}{\partial y^2} - \frac{1}{D_f + D}\frac{\partial w}{\partial t} = 0 \tag{D5}$$

with initial and boundary conditions given by equations (D6) and (D7), which for this case are

$$\left.\begin{aligned} w(y,0) &= M(y) - \frac{fY}{2(D_f + D)}\left(y_2^2 - y^2\right) \\ w(y_2) &= 0 \\ \frac{\partial w}{\partial y} &= 0 \quad \text{at} \quad y = 0 \end{aligned}\right\} \tag{D11}$$

Equation (D5) may be solved by separation of variables. Let $w(y,t)$ be given by

$$w(y,t) = G(y)H(t) \tag{D12}$$

By differentiation, equation (D5) becomes

$$\left.\begin{aligned} H\frac{d^2G}{dy^2} - \frac{G}{D_f + D}\frac{dH}{dt} &= 0 \\ \text{or} \\ \frac{d^2G/dy^2}{G} = \frac{dH/dt}{H(D_f + D)} &= -\beta^2 \end{aligned}\right\} \tag{D13}$$

The general solutions to these equations are

$$\left.\begin{aligned} H &= a_1 e^{-(D_f+D)\beta^2 t} \\ \text{and} \\ G &= a_2 \sin \beta y + a_3 \cos \beta y \end{aligned}\right\} \tag{D14}$$

but since by condition (D11)

$$\frac{\partial w}{\partial y} = 0 \qquad \text{at} \quad y = 0$$

$a_2 = 0$ and $w(y,t)$ is then equal to

$$w(y,t) = a_4 e^{-(D_f+D)\beta^2 t} \cos \beta y \tag{D15}$$

where

$$a_4 = a_1 a_3$$

Another boundary condition (D11) is

$$w(y_2) = 0$$

or

$$a_4 \cos \beta y_2 = 0 \tag{D16}$$

The values of β for which this is true are given by

$$\beta_n = \frac{2n+1}{2} \frac{\pi}{y_2} \qquad n = 0, 1, 2 \ldots \tag{D17}$$

Thus, the solution (D15) becomes

$$w(y,t) = \sum_{n=0}^{\infty} a_n e^{-(D_f+D)\beta_n^2 t} \cos \beta_n y \tag{D18}$$

where the terms form an orthogonal system. The constants a_n can be found by using initial condition (D11), which gives

$$w(y,0) = M(y) - \frac{fY\left(y_2^2 - y^2\right)}{2(D_f + D)} = \sum_{n=0}^{\infty} a_n \cos \beta_n y \tag{D19}$$

from which we obtain

$$a_n = \frac{\int_0^{y_2} \left[M(y) - \frac{fY\left(y_2^2 - y^2\right)}{2(D_f + D)} \right] \cos \beta_n y \, dy}{\int_0^{y_2} \cos^2 \beta_n y \, dy} \tag{D20}$$

Integrating equation (D20) gives

$$a_n = \frac{2}{y_2} \int_0^{y_2} M(y) \cos \beta_n y \, dy - \frac{2fY(-1)^n}{y_2 \beta_n^3 (D_f + D)} \tag{D21}$$

The concentration $c(y, t)$ can then be obtained by combining equations (D3), (D10), (D18), and (D21).

$$c(y,t) = \sum_{n=0}^{\infty} \left[\frac{2}{y_2} \int_0^{y_2} M(y) \cos \beta_n y \, dy - \frac{2fY(-1)^n}{y_2 \beta_n^3 (D_f + D)} \right] \left[e^{-(D_f + D)\beta_n^2 t} \cos \beta_n y \right]$$

$$+ \frac{fY}{2(D_f + D)} \left(y_2^2 - y^2 \right) \tag{D22}$$

Special Case - Zero Initial Concentration

The initial condition for this special case is given by equation (D8)

$$M(y) = 0 \tag{D8}$$

Applying this condition to equation (D22) gives

$$c(y,t) = \frac{fY}{2(D_f + D)}\left[y_2^2 - y^2 - \frac{4}{y_2}\sum_{n=0}^{\infty}\frac{(-1)^n e^{-(D_f+D)\beta_n^2 t}\cos\beta_n y}{\beta_n^3}\right]$$

which, if rearranged slightly, yields

$$c(y,t) = \frac{fYy_2}{2(D_f + D)}\left[1 - \frac{y^2}{y_2} - \frac{32}{\pi^3}\sum_{n=0}^{\infty}\frac{(-1)^n \cos\beta_n y\, e^{-(D_f+D)\beta_n^2 t}}{(2n+1)^3}\right] \tag{D23}$$

Equation (D23) is equivalent to the heat-transfer solution presented by Carslaw and Jaeger (ref. 19, p. 130). The release rate from the fuel is related to the concentration gradient at the fuel surface by equation (C5)

$$r = \frac{KYSLf}{4} - (D_f + D)S\left.\frac{dc}{dy}\right|_{y_2} \tag{C5}$$

where

$$\left.\frac{dc}{dy}\right|_{y_2}$$

is obtained by differentiation of (D23). The release rate is

$$r = \frac{KYSLf}{4} + fYy_2S\left[1 - \frac{8}{\pi^2}\sum_{n=0}^{\infty}\frac{e^{-(D_f+D)\beta_n^2 t}}{(2n+1)^2}\right] \tag{D24}$$

The total amount of gas released from $t = 0$ to $t = t$ is found by direct integration of equation (D24):

$$r_T = \int_0^t r\,dt = \frac{KYSLft}{4} + fYy_2S\left[t + \frac{8}{\pi^2}\sum_{n=0}^{\infty}\frac{e^{-(2n+1)^2\alpha} - 1}{(2n+1)^4\frac{\alpha}{t}}\right] \tag{D25}$$

where we have defined

$$\alpha \triangleq (D_f + D)\pi^2\frac{t}{4y_2^2}$$

This result can be expressed in the form

$$\frac{\text{Total release}}{\text{Total birth}}$$

by dividing by $B = fYy_2St$, which then gives

$$\frac{r_T}{B} = \frac{KL}{4y_2} + 1 - \frac{8}{\pi^2}\sum_{n=0}^{\infty}\frac{1 - e^{-(2n+1)^2\alpha}}{(2n+1)^4\alpha} \tag{D26}$$

Equations (D24), in terms of $r(t)/r(t = \infty)$, and (D26), neglecting recoil, are plotted in terms of α in figure 29.

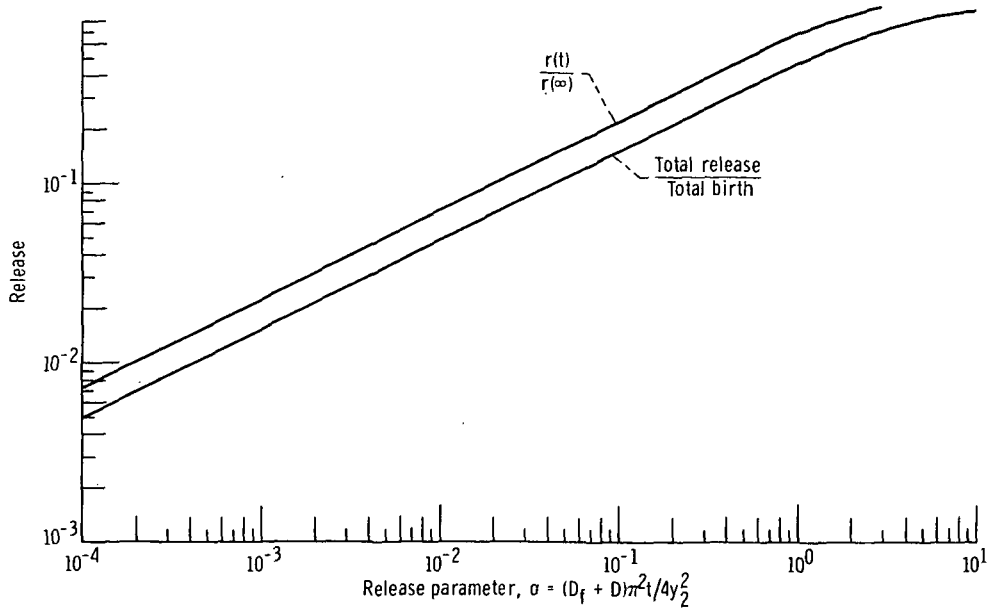

Figure 29. - Diffusional release from a slab.

Special Case - Step Change in Conditions

This solution corresponds to a step change in fuel operating conditions ($D_f \rightarrow D_f'$, $D \rightarrow D'$, $f \rightarrow f'$) after operating for some time τ starting at an initial concentration of zero.

For this case, the concentration $M(y)$ is given by equation (D23). The concentration $c(y,t)$, where t is now the operating time after the step change at τ, is found by combining equation (D22) with (D23), where D, D_f, and f have been replaced by D', D_f', and f':

$$c(y,t) = \sum_{n=0}^{\infty} \left[\frac{2}{y_2} \int_0^{y_2} M(y) \cos \beta_n y \, dy - \frac{2f'Y(-1)^n}{y_2 \beta_n^3 (D_f' + D')} \right] \left[e^{-(D_f'+D')\beta_n^2 t} \cos \beta_n y \right]$$

$$+ \frac{f'Y}{2(D_f' + D')} \left(y_2^2 - y^2 \right) \qquad \text{(D22)}$$

$$M(y) = \frac{fYy_2^2}{2(D_f + D)}\left[1 - \frac{y^2}{y_2^2} - \frac{32}{\pi^3}\sum_{i=0}^{\infty}\frac{(-1)^i \cos \beta_i y\, e^{-(D_f+D)\beta_i^2 \tau}}{(2i+1)^3}\right] \tag{D23}$$

and the summation index has been changed to i. Integration yields equation (D27)

$$c(y,t) = \sum_{n=0}^{\infty}\left\{\frac{2fY(-1)^n\left[1 - e^{-(D_f+D)\beta_n^2\tau}\right]}{y_2(D_f + D)\beta_n^3} - \frac{2f'Y(-1)^n}{y_2\beta_n^3(D_f' + D')}\right\}\left[e^{-(D_f'+D')\beta_n^2 t}\cos \beta_n y\right]$$

$$+ \frac{f'Y\left(y_2^2 - y^2\right)}{2(D_f' + D')} \tag{D27}$$

The release rate is again obtained from equation (C5)

$$r = \frac{KYSLf'}{4} - (D_f' + D')S\left.\frac{dc}{dy}\right|_{y_2} \tag{C5}$$

which yields

$$r = \frac{KYSLf'}{4} + f'Yy_2S + \sum_{n=0}^{\infty}(D_f' + D')S\left\{\frac{2fY\left[1 - e^{-(D_f+D)\beta_n^2\tau}\right]}{y_2(D_f + D)\beta_n^3}\right.$$

$$\left. - \frac{2f'Y}{y_2\beta_n^3(D_f' + D')}\right\}\beta_n e^{-(D_f'+D')\beta_n^2 t} \tag{D28}$$

APPENDIX E

SYMBOLS

A	activity, disintegrations/cm^3-sec
A_1	activity of isotope 1, disintegrations/sec
A_2	activity of isotope 2, disintegrations/sec
a	constant
a_n	constant coefficients
B	total birth (atoms formed by fissions), atoms
b	burnup, percent uranium atoms fissioned
c	concentration of fission products, atoms/cm^3
D	diffusion coefficient, cm^2/sec
D'	diffusion coefficient for second time step
D_f	fission-enhanced-diffusion coefficient, cm^2/sec
D_f'	fission-enhanced-diffusion coefficient for second time step
D_o	diffusion constant, cm^2/sec
D_{fo}	fission-enhanced-diffusion constant, cm^2/sec
d	combination of terms, KT
E	combination of terms, $\lambda/(D_f + D)$
F	combination of terms, $fY/(D_f + D)$
f	fission-rate density, fissions/cm^3-sec
f'	fission-rate density for second time step
G	a function of y, defined by eqs. (D12) and (D13)
H	a function of t, defined by eqs. (D12) and (D13)
h	gas gap thickness, cm
K	fraction of recoils stopped by gas after ejection
L	recoil length in fuel, cm
ℓ	recoil length in gas, cm
M	initial concentration in fuel, atoms/cm^3

N	surface concentration, atoms/cm^3
Q	energy of activation for diffusion, J/mole
$\dot{Q}$	volumetric flow rate, cm^3/sec
R	gas constant, 8.314 J/mole-K
r	release rate, atoms/sec
r_o	release rate at time equals zero, atoms/sec
r_T	total release, atoms
S	surface area, cm^2
T	temperature, K
t	operating time, sec
u	a concentration function, defined by eq. (D4)
V	sweep gas system flow volume, cm^3
w	a concentration function, defined by eq. (D5)
Y	fractional fission yield, atoms/fission
y	thickness, cm
y_1	slab thickness, cm
y_2	slab half thickness, cm
α	release parameter, $(D_f + D)\pi^2 t/4y_2^2$
β	a constant
β_n	eigenvalues, defined by eq. (D17)
λ	decay constant, sec^{-1}
τ	operating time, total time for first set of conditions, sec

REFERENCES

1. Nelson, R. S.: The Influence of Irradiation on the Nucleation of Gas Bubbles in Reactor Fuels. J. Nucl. Mat., vol. 25, no. 2, Feb. 1968, pp. 227-232.

2. Carroll, R. M.: Fission-Gas Effects in Reactor Fuels - Part I. Basic Studies. Nucl. Safety, vol. 12, no. 4, July-Aug. 1971, pp. 297-305.

3. Carroll, R. M.: Fission-Gas Effects in Reactor Fuels - Part II. Engineering Applications. Nucl. Safety, vol. 12, no. 6, Nov.-Dec. 1971, pp. 562-568.

4. Nichols, F. A.: Kinetics of Diffusional Motion of Pores in Solids. J. Nucl. Mat., vol. 30, no. 1/2, Apr. 1969, pp. 143-165.

5. Carroll, R. M.; and Sisman, O.: Evaluating Fuel Behavior During Irradiation by Fission-Gas Release. Rep. ORNL-4601, Oak Ridge National Lab., Sept. 1970.

6. Kirchgessner, Thomas A.; Weinstein, Michael B.; and Tambling, Thomas N.: A Sweep Gas Facility for Fission Gas Release Studies at the NASA Plum Brook Reactor. NASA TM X-2267, 1971.

7. Tennery, V. J.; Godfrey, T. G.; and Potter, R. A.: Synthesis, Characterization, and Fabrication of UN. Rep. ORNL-4608, Oak Ridge National Lab. (NASA CR-72764), Dec. 1970.

8. Carroll, R. M.; and Sisman, O.: In-Pile Fission-Gas Release From Single-Crystal UO_2. Nucl. Sci. Eng., vol. 21, no. 2, Feb. 1965, pp. 147-158.

9. Belle, Jack, ed.: Uranium Dioxide: Properties and Nuclear Applications. Naval Reactors, Division of Reactor Development, U.S. Atomic Energy Commission, 1961.

10. Fulmer, C. B.: Density Effect on Energy versus Range of Fission Fragments in Gases. Phys. Rev., vol. 139, no. 1B, July 1965, pp. 54-55.

11. Evans, Robley D.: The Atomic Nucleus. McGraw-Hill Book Co. Inc., 1955.

12. Keller, Donald L.: Progress on Development of Fuels and Technology for Advanced Reactors During July 1970 Through July 1971. Rep. BMI-1918, Battelle Columbus Lab., July 1971.

13. Wohn, F. K.; Talbert, W. L., Jr.; and Halbig, J. K.: The Decay of ^{85m}Kr. Nucl. Phys., vol. A152, 1970, pp. 561-569.

14. Lycklama, H.; Archer, N. P.; and Kennett, T. J.: Beta Decay of ^{87}Kr, ^{88}Kr, and ^{88}Rb. Can. J. Phys., vol. 47, no. 4, Feb. 15, 1969, pp. 393-409.

15. Bocquet, J. P.; Brissot, R.; Crancon, J.; Pinston, J. A.; Schussler, F.; and Moussa, A.: Désintégration Du ^{87}Kr. Nucl. Phys., vol. A125, 1969, pp. 613-625.

16. Onega, Ronald J.; and Carpenter, William B.: The Decay Scheme of ^{87}Kr. Nucl. Phys., vol. A137, 1969, pp. 211-221.

17. Lycklama, H.; and Kennett, T. J.: Level Structure of ^{88}Rb. Can. J. Phys., vol. 48, no. 6, Mar. 15, 1970, pp. 753-758.

18. Trammell, M. R.; and Henninger, W. A.: Nuclear Data Library for the Fission Product Program. Rep. WANL-TME-574 (Rev. 1), Westinghouse Astronuclear Lab., Nov. 17, 1966.

19. Carslaw, H. S.; and Jaeger, J. C.: Conduction of Heat in Solids. Second ed., Clarendon Press, 1959.

NASA-Langley, 1973 — 22 E-7097

Page Intentionally Left Blank

NATIONAL AERONAUTICS AND SPACE ADMINISTRATION
WASHINGTON, D.C. 20546

OFFICIAL BUSINESS
PENALTY FOR PRIVATE USE $300

SPECIAL FOURTH-CLASS RATE
BOOK

POSTAGE AND FEES PAID
NATIONAL AERONAUTICS AND
SPACE ADMINISTRATION
451

U.S.MAIL

POSTMASTER : If Undeliverable (Section 158 Postal Manual) Do Not Return

"The aeronautical and space activities of the United States shall be conducted so as to contribute . . . to the expansion of human knowledge of phenomena in the atmosphere and space. The Administration shall provide for the widest practicable and appropriate dissemination of information concerning its activities and the results thereof."

—NATIONAL AERONAUTICS AND SPACE ACT OF 1958

NASA SCIENTIFIC AND TECHNICAL PUBLICATIONS

TECHNICAL REPORTS: Scientific and technical information considered important, complete, and a lasting contribution to existing knowledge.

TECHNICAL NOTES: Information less broad in scope but nevertheless of importance as a contribution to existing knowledge.

TECHNICAL MEMORANDUMS: Information receiving limited distribution because of preliminary data, security classification, or other reasons. Also includes conference proceedings with either limited or unlimited distribution.

CONTRACTOR REPORTS: Scientific and technical information generated under a NASA contract or grant and considered an important contribution to existing knowledge.

TECHNICAL TRANSLATIONS: Information published in a foreign language considered to merit NASA distribution in English.

SPECIAL PUBLICATIONS: Information derived from or of value to NASA activities. Publications include final reports of major projects, monographs, data compilations, handbooks, sourcebooks, and special bibliographies.

TECHNOLOGY UTILIZATION PUBLICATIONS: Information on technology used by NASA that may be of particular interest in commercial and other non-aerospace applications. Publications include Tech Briefs, Technology Utilization Reports and Technology Surveys.

Details on the availability of these publications may be obtained from:

SCIENTIFIC AND TECHNICAL INFORMATION OFFICE

NATIONAL AERONAUTICS AND SPACE ADMINISTRATION

Washington, D.C. 20546